Journal of Materials Chemistry B

ROYAL SOCIETY OF CHEMISTRY

PAPER

View Article Online
View Journal

Published on 14 July 2025. Downloaded by Indian Institute of Technology New Delhi on 8/9/2025 1:57:37 AM.

Check for updates

Cite this: DOI: 10.1039/d5tb01126d

# A 3D bioprinted *in vitro* full-thickness skin aging model

Juhi Chakraborty, Abhishak C. Gupta and Sourabh Ghosh *

Received 11th May 2025,
Accepted 1st July 2025

DOI: 10.1039/d5tb01126d

rsc.li/materials-b

Aging is caused by numerous factors resulting in physiological modification, affecting skin functionality. Developing an *in vitro* aging skin model is difficult since aging is a complex and cumulative activity throughout a person's lifetime. Moreover, skin is composed of multiple cell types; hence, it is challenging to replicate this intricate phenomenon quickly. Here, we report the development of a 3D bioprinted skin aging model using silk fibroin–gelatin bioink recapitulating the dual layer of the epidermis and dermis, along with a focus on the dermal–epidermal junction present in the native aged skin. We exploited the use of the senescent/late passage fibroblasts and keratinocytes in co-culture. This was compared with the proliferative/early passage cells as a control. Reduced fibronectin expression in gene and protein analysis, accompanied by a decline in collagen I, II, and IV expression, demonstrates the potency of our model in recapitulating the attributes of extrinsic aging *in vitro*. In addition, we created two diseased conditions – oxidative stress brought on by $H_2O_2$ and elevated glucose, as potential substitute agents for senescence induction. While both conditions were effective as alternate methods of inducing aging, high glucose was found to have more potency. Our developed 3D bioprinted skin aging model has numerous uses in basic research on aging, disease modeling, and screening of pharmaceutical active ingredients.

## 1. Introduction

Aging is an inevitable outcome resulting from the cellular damage accumulated over time.[1] In humans, aging is characterized by many changes at both the cellular and molecular levels. A decline in mitochondrial functioning, oxidative stress, alteration in the constitution of the proteins in the extracellular matrix (ECM), and an alteration in gene expression contribute to aging (Fig. 1A).[2] Another widely known mechanism linked to aging is telomerase, a ribonucleoprotein in the absence of which somatic cells fail to sustain the telomeric DNA.[3] Most aging-related research is determined by the prerequisite of understanding its mechanism in humans. While studying the aging process, the prime matter of concern is the requirement of cells and tissues, and the need to have deep monitoring over these systems in an organism for an extended period, essentials that are not achievable in humans. Instead, studying the aging mechanism in a model system enables us to find an equilibrium between the practicality on the one hand and the need for the system to be biologically relevant on the other hand.[4] Surprisingly, the number of experimental models available to investigate the mechanism of aging and its involvement in diseases is limited.

Several attempts have been undertaken to develop aging models *in vivo* and *in vitro* to understand the cellular signaling mechanism, cell–cell, cell–matrix interaction, and the process of different types of disease progression. For example, aged (120 days) and young (60 days) rat models were subjected to sepsis to investigate the neurochemical and behavioral parameters.[5] This study concluded that aging slightly influenced septic rats' brain inflammation and behavioral changes. In a similar study, Herbig *et al.*[6] studied telomere dysfunction in baboons. They reported a gradual increase in the senescent fibroblasts in the aging skin, which was confirmed by the heterochromatinized nuclei and the presence of ataxia-telangiectasia muted kinase. Although the studies carried out *in vivo* could achieve nominal success, the investigative research often ends with a failure while translating the promising results, primarily due to the variation in the immune response and skin architecture between the short-lived lower animals and the longer-lived higher mammals. Secondly, genetic manipulations feasible in laboratory animals can seldom be applied directly to humans,[7] making it difficult to match the aging mechanisms in animals to those in humans. Moreover, skin aging research also correlates with the testing of cosmetic products; however, the European Union has banned testing cosmetic products or any pharmaceuticals on animals. These apparent reasons, high cost, and time consumption have compelled researchers to look for alternative *in vitro* methods.

*Department of Textile and Fibre Engineering, Indian Institute of Technology Delhi, New Delhi-110016, India. E-mail: Sourabh.Ghosh@textile.iitd.ac.in*

Published on 14 July 2025. Downloaded by Indian Institute of Technology New Delhi on 8/9/2025 1:57:37 AM.

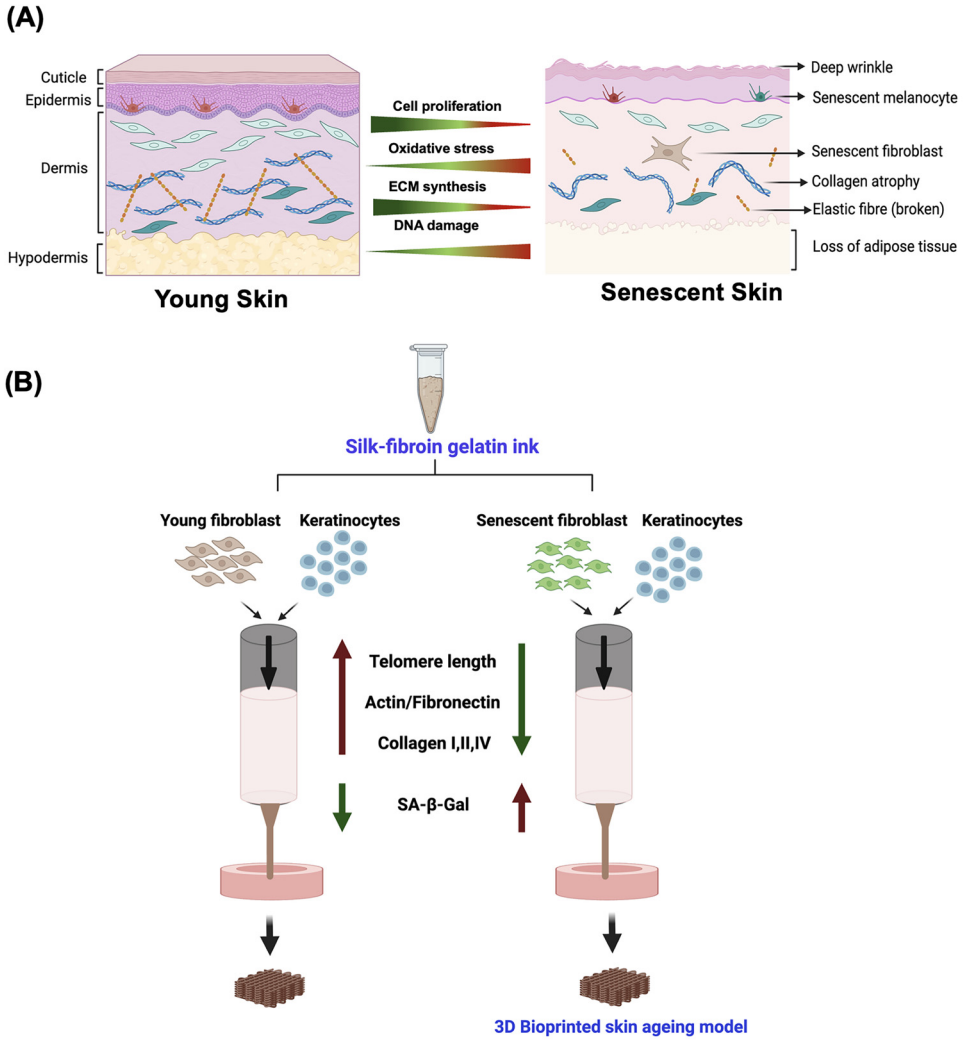


Fig. 1 Schematic representation (A) of the difference between the young and senescent skin, with an arrow gradient depicting the changes at the cellular level, and (B) followed towards the development of a 3D bioprinted skin aging model [Created with BioRender.com].

At present, three-dimensional (3D) skin aging equivalents are reconstructed and used as a potential substitute to the animal aging model. Initially, the 3D culture system was established by culturing human dermal fibroblasts (HDFs) and epidermal keratinocytes on collagen gel[8] and nylon mesh carriers.[9,10] Currently, various upgraded skin aging models are available commercially,[11,12] for instance, the Phenion® FT Aged Skin Model, developed by Henkel, is an excellent tool for studying the molecular aging pathways since it structurally and physiologically resembles aged human skin.[13] Lago *et al.*,[14] for instance, employed three separate *in vitro* aging models (i) by treating HDF cells with UV-B irradiation, and (ii) proliferative HDFs obtained from aged and (iii) young donors. They reported altered gene expression levels in fibroblasts during the aging process in all three models and reduced cell growth. This indicates that their model could successfully be used to understand the aging mechanism and be used for drug screening. In a similar study, Santos *et al.*[15] investigated the epidermis's chronological aging by developing an *in vitro* 3D model of skin aging that displayed age-related characteristics such as decreased hyaluronan expression and its surface receptor CD44 and a decrease in epidermal thickness. Even though this model closely resembles aged skin *in vivo*, the lengthy culture period required to generate it is a drawback for the high-throughput production of skin equivalents.[16] To overcome this obstacle, senescent cells, which cease to divide but continue functioning metabolically, have been directly incorporated into bioengineered skin models alongside other normal cells. This has allowed for a more accurate depiction of the skin micro-environment and the intricate relationships between all cells.[17] In another attempt to develop an *in vitro* skin aging model, Jeong *et al.*[18] developed a flexible skin-on-a-chip and applied mechanical compression to mimic the circadian rhythm to accelerate the aging process. Although reduced epidermal thickness, contraction rate, and release of Myb, a transcription factor that is essential for preserving skin homeostasis, whose dysregulation can accelerate the aging process of the skin,[19] were indicators of accelerated aging linked to periodic

 This journal is © The Royal Society of Chemistry 2025

Published on 14 July 2025. Downloaded by Indian Institute of Technology New Delhi on 8/9/2025 1:57:37 AM.

compressive stress, however, the study failed to replicate the epidermal–dermal crosstalk present in the native aged skin. To overcome this challenge, Lee *et al.*[20] were the first to bioprint two separate cell layers, inner fibroblasts and outer keratinocytes, to produce a 3D collagen hydrogel structure that resembles stratified skin. Baltazar *et al.*[21] reported using a skin substitute using 3D bioprinting that excludes the need for skin grafts in mice. By using human endothelial cells along with human placental pericytes, this synthetic multilayered graft created microvascular networks that, when implanted into the mouse dorsum, showed perfusion *in vivo*. In this model, keratinocytes from the human foreskin were used as the epidermis, with fibroblasts and endothelial cells suspended in collagen. This kind of skin substitute is thought to improve wound healing by improving site-specific conformance, increasing vascularization, and removing the requirement for graft harvest. Despite these reported studies being an efficient alternative to animal testing, *in vitro* models are limited because they fail to imitate the full human aging skin, comprising different cell types and the dermal–epidermal junction (DEJ) known as rete ridges. Hence, to investigate the efficacy of the natural anti-aging extracts, pharmaceuticals, and cosmetics, we need more human cell-based models to replicate the full-thickness architecture of the aged human skin.

One of the critical factors contributing to aging is the cellular senescence of the cells derived from the dermis which causes retardation of growth due to a diminished proliferative ability of cells that usually arises from the intrinsic aging process. Akin to all organs, replicative senescence that occurs with age is also reflected in dermal fibroblasts.[22] A decline in the replicative capacity of the HDFs occurs in culture after a fixed number of population doublings, which is extensively used as an *in vitro* senescence model.[23] Generally, senescent cells are larger than young ones and grow to a lesser saturation density.[24] This constrained lifespan *in vitro* has resulted in the substantial application of HDFs as a model system for studying the process of human cellular aging. Fabrication of a successful 3D skin aging model that simulates the architecture of the aged human skin could be achieved by targeting the following features: (i) establishing epidermal–dermal crosstalk, which is essential for the maintenance of skin homeostasis,[12] and (ii) employing pristine cell lines and not the ones which have been kept for an extended period in culture.[25] The introduction of 3D bioprinting can make a paradigm change in skin tissue engineering by providing opportunities for automated production of structurally sophisticated and physiologically comparable human skin counterparts. 3D bioprinting enables high precision and reproducibility with respect to controlled architecture (in terms of size, form, geometry, and orientation), while also allowing possibilities to use various bioink materials and cell types.[26–28] Furthermore, it offers numerous benefits, including the capacity to fully replicate a functional human skin equivalent, removing the need for animal testing.[29] The capacity to recreate patient-specific tissues tailored to fit the graft location during reconstructive surgery can reduce or eliminate post-procedural scarring.[30] Towards this end, in our previous study,[31] we reported the fabrication of a full-thickness skin equivalent construct using the 3D bioprinting strategy. The unique finding of the study was that our fabricated 3D bioprinted skin model was successful in replicating the undulated morphology present in the epidermal rete ridges as well as biochemical, mechanical, and architectural characteristics akin to the human skin, not achievable by monolayer-based cell culture techniques. In the present study, we explored the knowledge obtained from our previous study to fabricate a 3D bioprinted full-thickness skin aging model equivalent by using late passage HDF cells in co-culture with keratinocytes and comparing them with the early passage co-culture counterparts to assess various factors and signaling cascades related to aging. This was achieved by exploiting the effectiveness of the silk fibroin–gelatin (SF–G) bioink established previously.[31] Even though passage-dependent variation in aging research has gained much attention, whether the changes observed in the diploid cell population following serial passaging *in vitro* precisely resemble the human cellular aging process *in vivo* is still a big question.

Stress to the cells in the form of oxidative damage is another critical factor contributing to aging, such that the cells exit from the cell cycle in an irreversible manner and stop dividing.[32] Cellular senescence by oxidative stress has been considered a remarkable *in vitro* model for illustrating the molecular mechanisms involved in aging research.[33] Hydrogen peroxide ($H_2O_2$), an oxidant and a natural metabolite, originates from cellular respiration as a side product and from various cytokines and growth factors. It is extensively used to attain oxidative stress-induced premature senescence within a short period.[34] Exposure of HDFs to sublethal concentrations of $H_2O_2$ transforms them into a condition resembling senescence. Chen *et al.*[35] investigated the impact of oxidative damage on HDF cells. They treated the HDF F65 cells with $H_2O_2$ to establish an *in vitro* model capable of dictating the interrelationship of cellular damage, cessation of replication, and molecular response. In a similar study, Duan *et al.* treated young human diploid fibroblast cells with low doses of $H_2O_2$ for an extended period.[36] The cells irreversibly manifested cellular senescence through G1 cell cycle arrest and senescence-associated β-galactosidase. Higher glucose levels have been a significant determinant of premature cellular senescence. A higher incidence of various age-related diseases prevails in diabetic patients at a very early age compared with in healthy controls.[37] Multiple studies have reported that HDFs give rise to an elevated quantity of reactive oxygen species (ROS) under a hyperglycemic environment at the cellular level, resulting in an induction of cellular senescence prematurely in an enhanced manner.[38,39] Indeed, several research findings in both humans and lower model organisms have supported the fact that elevated levels of glucose function as an aging accelerator.[40] Many mechanisms have contributed to skin aging due to high glucose. One of them is the formation of advanced glycation end-products (AGEs), the final waste product generated in response to high glucose levels, resulting in cross-links in the collagen, thus resulting in premature aging.[41]

Published on 14 July 2025. Downloaded by Indian Institute of Technology New Delhi on 8/9/2025 1:57:37 AM.

Apart from collagen, elastin is also affected by AGEs, contributing to the loss of skin elasticity. Therefore, considering this, we induced aging in HDF using $H_2O_2$, a potent oxidative stress agent, and high glucose that impedes fibroblast proliferation, as it would be interesting to study the outcome of $H_2O_2$ and high glucose exposure on the fibroblast cells.

Hence, in the present study, we report the development of a 3D bioprinted aging skin model by exploring the early and late passage HDFs in co-culture with keratinocytes, thus simulating the epidermal and dermal layer of the native senescent skin (Fig. 1B). Next, we induced aging in the proliferative (early passage) HDFs using $H_2O_2$, one of the significant oxidative stresses, and high glucose, mimicking diabetic conditions, which are significant factors contributing to aging. We speculate that the aging model we developed will be highly effective in testing anti-aging cosmetics and drugs when compared to the traditional *in vitro* monolayer and animal models, and can successfully recapitulate the characteristics and functionality of native aged skin.

# 2. Materials and methods

## 2.1. Cell culture, expansion, and treatment

Primary adult HDFs were procured from Himedia (CL005) and expanded at a density of 6000 cells per $cm^2$ in minimum essential medium Eagle (Alpha modification, Himedia ALO80) supplemented with 10% fetal bovine serum (FBS) (Hyclone, SH30071.03), 100 U $mL^{-1}$ penicillin/streptomycin (Himedia, A001A), 2.5 μg $mL^{-1}$ of amphotericin B (Himedia, A011), 50 μg $mL^{-1}$ gentamycin, and 5 ng $mL^{-1}$ of FGF-2 (Prospec, Cyt-218-b), hereafter referred to as the fibroblast proliferation media.[31] Cells with passage numbers 6–8 were considered early passage, and 30–31 as late passage.

Primary adult human epidermal keratinocytes were obtained from Himedia (CL006) and expanded with a cell density of 6000 cells per $cm^2$ in media containing DMEM : F12 (1 : 1) mixture, adenine (180 μM), insulin (5 μg $mL^{-1}$), hydrocortisone (0.5 μg $mL^{-1}$), EGF-2 (10 ng $mL^{-1}$), cholera toxin (10 pg $mL^{-1}$), 100 U $mL^{-1}$ of penicillin–streptomycin, amphotericin (2.5 μg $mL^{-1}$), gentamicin (50 μg $mL^{-1}$), HEPES (1×) and FBS (10%), hereafter referred to as the keratinocyte proliferation media.[31]

Keratinocytes with passage numbers 6–8 were used for all the experiments of co-culture and 3D bioprinting. The early and late passage fibroblasts were expanded in T25 flasks for 3 days in fibroblast proliferation media to achieve the co-culture conditions. Keratinocytes were then added and expanded for 3 days in keratinocyte proliferation media. The mixture of cells was then kept in cornification media for 7 days.[31]

Stress-induced premature senescence was achieved by exposure to $H_2O_2$. Briefly, early passage fibroblasts ($3 \times 10^4$ cells per $cm^2$ in DMEM) were treated with a 200 μM concentration of $H_2O_2$ for a short period of 120 min and analyzed at different time points after exposure. The cells were propagated in a T-25 flask. For high glucose treatment, early passage fibroblasts ($3 \times 10^4$ cells per $cm^2$ in DMEM) were treated with 50 mM glucose and analyzed at different time points.

## 2.2. Preparation of silk fibroin (SF) solution

The SF solution from *Bombyx mori* cocoons was prepared as described previously.[31,42] Briefly, 5 g of silk cocoons were cut into smaller pieces, boiled twice in 0.02 M $Na_2CO_3$, and thoroughly rinsed with deionized water to remove alkali from the degummed fibers. The extracted fibers were dried overnight and dissolved using a 9.3 M LiBr solution (SRL Pvt. Ltd, India) at 60 °C for 4 h. The resultant fibroin solution was dialyzed against deionized water using the Slide-a-Lyzer dialysis cassette (MWCO 3500, Pierce, USA) for 48 hrs to remove LiBr, resulting in 5% w/v of SF aqueous solution.

## 2.3. Preparation of SF–G bioink

SF–G bioink was prepared following the protocol described previously.[31,42] Briefly, 5% of gelatin from porcine skin type A (Sigma-Aldrich) was dissolved in 5% autoclaved SF solution. Media supplements (10× concentrated Eagle's minimum essential medium, Sigma, M0275) and 10% fetal calf serum were added to support cellular activity. All components were mixed homogeneously and maintained at 37 °C until cells were added. For the dermal component, HDF was combined with the SF–G blend at a density of $2 \times 10^6$ cells per mL, and for the epidermal component, keratinocytes were mixed with the SF–G blend at a density of $5 \times 10^6$ cells per mL. 800 units per mL of mushroom tyrosinase (Sigma-Aldrich) was added to the bioink before printing to initiate cross-linking.

## 2.4. 3D CAD model and preparation of the 3D bioprinted construct

Robocad V 4.0 software (3D Inks LLC, OK, USA) was used to design the 3D CAD model to imitate the dermal and epidermal layers of aged human skin. An overall dimension of 6 mm × 25 mm was printed. The dermal layer was composed of 10 layers, followed by 5 layers of the epidermis, as mentioned earlier.[31] Briefly, the interfilament distance was set to 750 μm for the first 5 layers, followed by 1500 μm for the subsequent 5 layers to form a groove-like design for housing the upper epidermal layers. For the epidermal layers, the interfilament distance was adjusted to 1500 μm. For each layer, the interlayer vertical displacement was maintained at 80 μm. The dermal structure's alternating grooves contributed to developing a complementary structure that represents the undulated design of the DEJ.

The early and late passage HDF-laden SF–G bioink was filled in two sterile 3 mL syringes and fitted with a pneumatic piston. The air bubbles in the syringe were removed before gelling at 20 °C. The syringe was then fixed on the extrusion head connected with a pressure-controlled pneumatic pump. Extrusion was carried out using direct-write assembly (Fiber Align, Aerotech Inc., Pittsburgh, USA) through a 210 μm microcapillary nozzle using the parameters optimized in our previous study.[31] Printing was carried out at 21 ± 1 °C with a speed of 1 mm $s^{-1}$ and 15–25 psi pressure for the 10-layered dermal construct with a 2 mm final height. The bioprinted constructs were transferred into a 50 mm Petri dish. They were incubated

 This journal is © The Royal Society of Chemistry 2025

Published on 14 July 2025. Downloaded by Indian Institute of Technology New Delhi on 8/9/2025 1:57:37 AM.

at room temperature (RT) for 1 h before the addition of fibroblast proliferation media and incubated at 37 °C thereafter for 3 days. Post day 3, the epidermal layers were printed above the dermal layers. They were then incubated with a 1 : 1 mixture of fibroblast and keratinocyte proliferation media for 3 days. The resultant dual-layer 3D bioprinted construct was then dissected into 6 mm × 6 mm small constructs and transferred to an air–liquid interface in 12-well transwell inserts (pore size 0.3 μm) for 7 days. Fibroblast proliferation: cornification media in the ratio of 1 : 1 was used for the final incubation in the transwell insert.

### 2.5. Senescence-associated beta-galactosidase (SA-β-Gal) staining

SA-β-Gal staining was carried out on day 7 for the early and late passage HDFs as well as the early passage fibroblasts treated with $H_2O_2$ and high glucose using the senescence β-galactosidase staining kit (Cell Signaling Technology, 9860). The protocol was followed as instructed in the manual. Briefly, the cells were washed twice with 1× PBS and fixed with 1 mL of 1× fixative for 10–15 min at RT. They were then washed with 1× PBS twice, and 1 mL of the β-Gal staining solution was added to each well. The plate was incubated in a dry incubator (no $CO_2$) overnight. The cells were checked under the fluorescence microscope (Leica, DMi8) with the SA-β-Gal still on the plate. The optimum activity was detectable at pH 6.0.

### 2.6. Relative human telomere length quantification by qRT-PCR

The DNeasy Blood & Tissue Kit (Qiagen, 69504) was used to extract DNA from the cells under different experimental conditions according to the manufacturer's instructions. For the early and late passage HDF, DNA was isolated on day 7 and days 3, 7, and 14 for the $H_2O_2$ and high glucose-treated fibroblast cells. The absolute human telomere length quantification qPCR assay kit (Cell Science, 8918) was used to determine the telomere length by qRT-PCR following the manufacturer's protocol.[43] It offers 2 pairs of primers, one to amplify the telomere and another to amplify a single-copy reference on the genome.

### 2.7. Gene expression analysis

RNA was isolated using an RNA isolation kit from the cells cultured in different experimental groups at specific time points (Qiagen, 74106). For instance, on day 7 for the early and late passage HDFs, and on days 3, 7, and 14 for the $H_2O_2$ and high glucose-treated cells. For co-culture and 3D bioprinted constructs, RNA was isolated post-7 days in cornification media. In the case of the bioprinted group, the constructs were first digested with the protease XIV enzyme (Sigma, P5147) at a final concentration of 250 μg $mL^{-1}$ and incubated for 20 min at 37 °C to obtain a single-cell suspension. Cells were separated from the remaining gel debris by centrifugation at 1200 rpm for 10 min. RNA purity and concentration were determined using a Nanodrop 2000C (Thermo Scientific, Wilmington, USA) spectrophotometer. 100 ng RNA was reverse-transcribed into cDNA using the first-strand cDNA synthesis kit (ThermoScientific, K1612). Quantitative RT-PCR was conducted using SYBR Green Master Mix (Quantitect, 204074) and a Rotor Gene Q thermocycler (Qiagen), as mentioned in our previous study.[44] QuantiTect primers (Qiagen) were used to investigate the gene expression of the cells mentioned in Table 1. Glyceraldehyde 3-phosphate dehydrogenase (GAPDH) was used as a housekeeping gene. Cells cultivated in a 2D monolayer on day 0 were used as the reference for all calculations. The $2^{-(\Delta\Delta c(t))}$ method was used to calculate the relative expression level.

Table 1 List of genes investigated using qRT-PCR

| Gene name | Full name | Catalog number |
|---|---|---|
| FN | Fibronectin | QT00038024 |
| Col 1A1 | Collagen type I alpha 1 chain | QT00037793 |
| Col 2A1 | Collagen type II alpha 1 chain | QT00035683 |
| Col 4A4 | Collagen type IV alpha 1 chain | QT00037256 |
| MMP 1 | Matrix metallopeptidase 1 | QT00014581 |
| MMP 2 | Matrix metallopeptidase 2 | QT00088396 |
| MMP 13 | Matrix metallopeptidase 13 | QT00001764 |
| GAPDH | Glyceraldehyde 3-phosphate dehydrogenase | QT00079247 |

### 2.8. Immunofluorescence analysis

Immunofluorescence was carried out to evaluate the expression of fibronectin and actin in a 2D monolayer (day 7), co-culture (after day 7 in the cornification media), employing the already optimized protocol.[45] Furthermore, the expression of the cytokeratins (CK1, CK14) for keratinocytes in the co-culture condition was also determined following 7 days in the cornification media. In brief, permeabilization was performed using 0.1% Triton X-100 (Sigma), followed by blocking with 1% BSA (Sigma) and three consecutive washes in PBS. Incubation in primary antibodies: anti-fibronectin (1 : 200, Abcam), actin phalloidin (1 : 50, Abcam), anti-cytokeratin 1 (CK-1) (1 : 100, Abcam), and anti-CK14 (1 : 100, Abcam) was performed for 1 h at RT. After washing with PBS, 2D monolayer cells were incubated with Alexa Fluor 488 conjugated goat anti-mouse IgG antibody (1 : 200, Invitrogen), and Alexa Fluor 546 goat anti-mouse IgG (1 : 200, Invitrogen) for 1 h at RT. DAPI (Sigma Aldrich) was used for nuclear staining. Images were captured using an inverted microscope by a Leica TCS SP5 (Leica Microsystems).

### 2.9. Immunohistochemical analysis

3D bioprinted constructs (after 7 days in transwell) were embedded in optimal cutting temperature (OCT) compound (Kaltek Srl) and snap-frozen in liquid nitrogen. 12 μm-thick sections were cut, air-dried, and stored at −20 °C until immunohistochemical staining. Briefly, the slides were kept at RT, air-dried for 20 min, and fixed in 10% formaldehyde (Kaltek Srl) for 1 h. Then, samples were re-hydrated with Tris-buffered saline (TBS, Sigma-Aldrich), and the non-specific antigenic sites were blocked with a protein block serum-free (Dako) for 10 min at RT. Then, sections were incubated for 1 h at RT with monoclonal mouse anti-fibronectin (1 : 200, Abcam), and actin phalloidin (1 : 50, 143533; Abcam) diluted with TBS. After 3

Published on 14 July 2025. Downloaded by Indian Institute of Technology New Delhi on 8/9/2025 1:57:37 AM.

washing steps in PBS, sections were first incubated with multi-linked biotinylated secondary antibody and then with the alkaline phosphatase-conjugated streptavidin (Biocare Medical) at RT for 10 min, respectively. DAPI (Sigma Aldrich) was used for nuclear staining. The colorimetric reactions were developed using a Fast Red kit (Biocare Medical). Images were captured using an inverted microscope by a Leica TCS SP5 (Leica Microsystems).

### 2.10. Protein expression analysis

The 3D bioprinted construct that represents the aging skin model fabricated from the late and early passage HDFs in co-culture was collected in 1.5 mL Eppendorf tubes after day 7 in Transwell plates with 100 μL of lysis buffer (Tris–HCl–NaCl-Nonidet P-40-S DS, sodium fluoride (1 mM), sodium orthovanadate (1 mM), phenylmethylsulfonyl fluoride (1 mM), protease inhibitor cocktail (Sigma-Aldrich Italy, P83409, diluted 1 : 200) and immediately snap-frozen in liquid nitrogen. The 2D early and late passage HDFs and their co-cultures were also incubated in lysis buffer for 15 min and then centrifuged at 7000*g* at 4 °C for 15 min. Supernatants were collected, and the extracted proteins were quantified using the Pierce BCA Protein Assay kit (Thermo Fisher Scientific, USA), according to manufacturer instructions, and stored at −80 °C. 10 μg protein samples were run on 8% SDS PAGE, and the bands of interest were processed for trypsin digestion.[46] Matrix-assisted laser desorption/ionization-time of flight (MALDI-TOF) based mass spectrometric (MS) analysis was performed using a Bruker Daltonics Ultraflex MALDI TOF/TOF mass spectrometer (Bruker, Germany). Protein identification was performed using the MASCOT search engine (Matrix Science) based on the MASCOT probability-based score using the SwissProt database selecting *Homo sapiens* taxonomy.

Furthermore, the interactions between the proteins coded by the differentially regulated genes were determined by the STRING V 10.0, a database of predicted and known protein interactions (**https://string-db.org/**). These interactions were determined to comprehend how the early/late passage HDFs in the 3D bioprinted constructs exhibited protein expression concerning the aging characteristics.[47]

### 2.11. HSC DNA damage

A HSC DNA damage immunostaining kit (Invitrogen, H 10292) was used to determine the DNA damage and the cytotoxicity of the HDF cells upon treatment with $H_2O_2$ and high glucose on day 7. 50 μL of Image-iT® Dead Green™ viability stain was added to treated cells and incubated for 30 min. The medium was removed, and cells were fixed in 4% formaldehyde at RT for 20 min. Permeabilization was performed using 0.1% Triton X-100 (Sigma), followed by blocking with 1% BSA (Sigma) and three consecutive washes in PBS. The cells were incubated with anti-γH2AX antibody (1 : 500) for 1 h at RT. After washing in PBS thrice, Alexa Fluor 546 goat anti-mouse IgG (1 : 200, Invitrogen) secondary antibody was added, and the cells were incubated for 1 h at RT, followed by Hoechst 33342 nuclear counterstain solution for 1 h in the dark. The cells were then washed with PBS thrice, and images were captured using an inverted microscope in a Leica TCS SP5 (Leica Microsystems).

### 2.12. Cell cycle analysis by FACS

$H_2O_2$ and high glucose-treated HDFs for 24, 48, and 72 h were prepared as a single-cell suspension in the buffer (*e.g.*, PBS + 2% FBS; PBS + 0.1% BSA) and fixed with cold 70% ethanol added dropwise while gently vortexing. The cells were fixed for at least 1 h at 4 °C. After washing properly with PBS, 1 mL of propidium iodide (PI) staining solution was mixed well with the cell pellet. Furthermore, 50 μL of RNase A stock solution (final concentration 0.5 μg $mL^{-1}$) was added and incubated overnight (or at least 4 hours) at 4 °C, and stained cells were then analyzed by flow cytometry (FACS BD).

### 2.13. Statistical analysis

The data were illustrated as mean ± SD and investigated using one-way ANOVA followed by Bonferroni's multiple comparison tests with '*n*' as the number of different experiments. The differences at $p < 0.05$(*), $p < 0.01$(**), $p < 0.001$(***) and $p < 0.0001$(****) were considered significant. Statistical analysis was done using GraphPad Prism (5.01), San Diego, California, USA.

## 3. Results

### 3.1 3D bioprinted skin aging model

**3.1.1 Features of the early and late passage HDF cells.** The early passage HDFs were uniform in shape and size (Fig. 2A(a)). In contrast, the late passage (senescent) cells were more prominent, flattened, and exhibited lamellopodia (Fig. 2A(b)). A decrease in the cell number was observed in the late passage HDFs on day 7 compared to their early passage counterpart (Fig. 2C(a)). Early and late passage HDFs in culture were treated with SA-β-gal, and their visible morphological features were investigated microscopically before and after treatment. Cytochemically detectable β-gal activity has been widely used as a marker of cellular senescence both *in vitro* and *in vivo*.[48] Observable differences were evident in both the fibroblast types upon treatment with SA β-gal. Senescent fibroblasts showed specific staining as a blue product (Fig. 2A(d)) of β-gal activity absent in proliferative or early passage cells (Fig. 2A(c)). The senescent activity escalated several-fold compared to the early passage ones when carried out at pH 6.0. A significant shortening of telomere length (2-fold) in late passage fibroblast cells ($p < 0.05$) was observed on day 7 compared to that of the early passage ones (Fig. 2C(d)).

Immunofluorescence (IFC) analysis was carried out to determine the expression of fibronectin and actin in the early and late passage HDF. Prominent expression of actin (Fig. 2B(a and d)) and fibronectin (Fig. 2B(b and d)) was observed in the early passage cells in a 2D monolayer. However, in the cytoplasm of late passage HDFs, both the protein types exhibited a distributed and decreased expression (Fig. 2B(e, f and h)). A large number of the nuclei were evident by the DAPI staining

 This journal is © The Royal Society of Chemistry 2025

Published on 14 July 2025. Downloaded by Indian Institute of Technology New Delhi on 8/9/2025 1:57:37 AM.

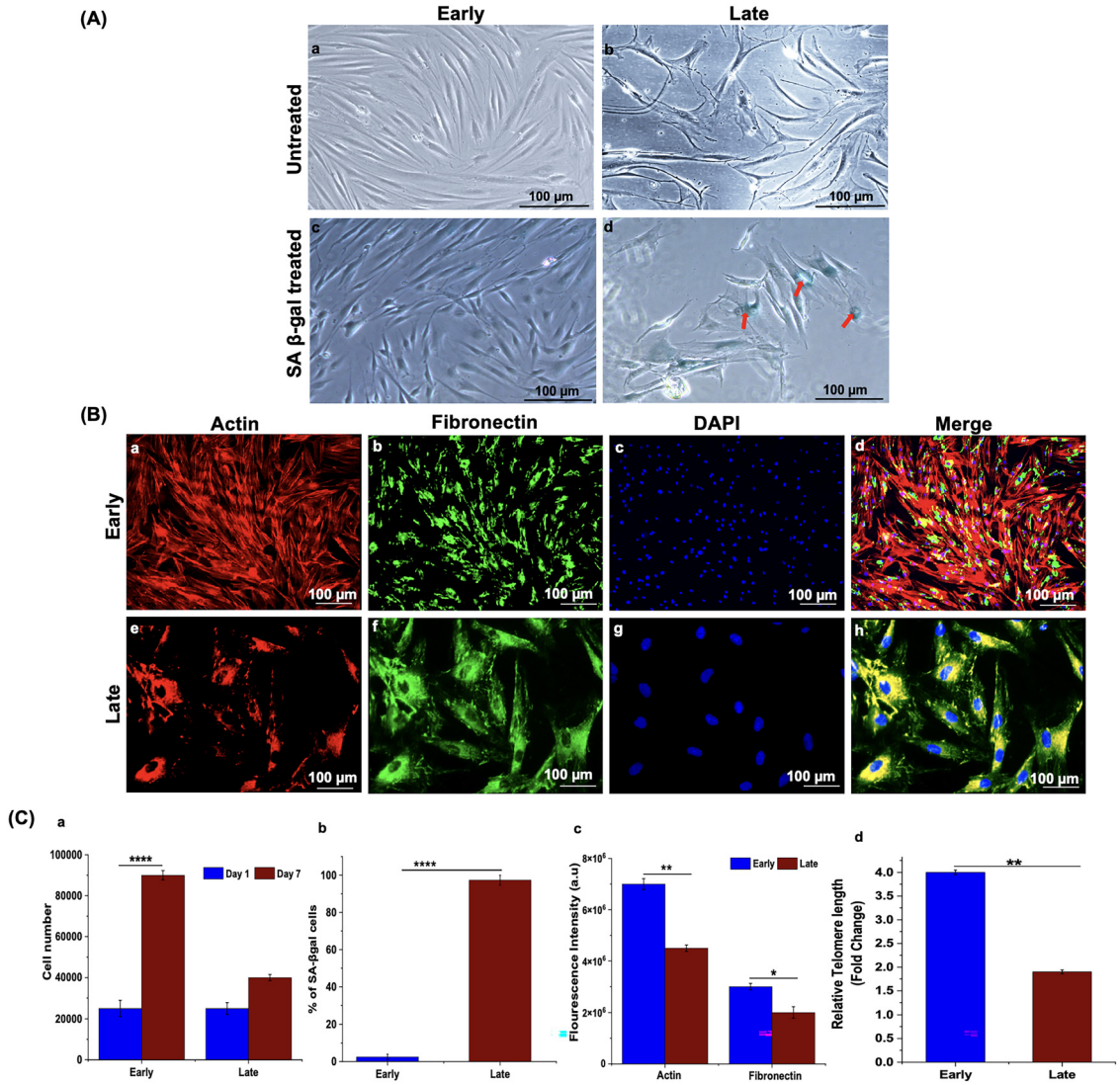


Fig. 2 (A) Bright field microscopic images depicting the morphology of (a) and (b) early and late passage fibroblast cells before; and (c) and (d) after staining with senescence-associated (SA) β-galactosidase on day 7; (B) immunofluorescence analysis depicting the protein expression of actin and fibronectin in early (a)–(d) and late passage (e)–(h) fibroblast cells on day 7 in 2D monolayer culture. (C) (a) Graphical representation of the cell number of the early and late passage fibroblast cells on day 1 and 7, (b) quantification of (SA) β-galactosidase expression of the early and late passage fibroblast cells on day 7, (c) fluorescence intensity comparison graphs, and (d) quantification of relative telomere length of the early and late passage fibroblast cells on day 7. Data represented as mean ± SD, significant at $p < 0.0001$.

(Fig. 2B(c)). Overall, the highest actin and fibronectin expressions were observed in early passage HDFs (Fig. 2C(c)) compared with their late passage counterparts.

**3.1.2 Baseline expression of the early and late passage fibroblasts and their co-culture.** The genes investigated were categorized according to their impact on the aging process: fibronectin which is an ECM component, COL 1A1, and COL 2A1 are responsible for collagen synthesis; COL 4A4 is particularly synthesized in the basement membrane, MMP 1, MMP 2, and MMP 13, the matrix metalloproteinases are accountable for the degradation of the proteins present in the ECM.[14] The gene expression levels were determined employing the ΔΔCt method.[49]

A significant expression of the major ECM protein fibronectin was observed in the early and late passage HDFs on day 7 and their co-culture condition after 7 days in cornification media. A decrease of less than 1-fold (Fig. 3A(a)) and 1.2-fold (Fig. 3B(a)) was observed in the late passage fibroblast and their co-culture compared to their early passage counterparts. The baseline expression supports the results obtained from the IFC analysis. A similar result was obtained with the COL1A1, where a 1-fold drop (Fig. 3A(b)) in the late passage and more than 2-fold (Fig. 3B(b)) in their co-culture was observed compared to the early passage cells. Whereas with another collagen type, COL 2A1 and COL 4A4 showed a non-significant expression both in the baseline (Fig. 3A(c and d)) and in co-culture (Fig. 3B(c and d)). Although there was an increase in the expression of MMP 2 in late passage fibroblasts (Fig. 3A(f)), the expression level was insignificant compared to the early

Published on 14 July 2025. Downloaded by Indian Institute of Technology New Delhi on 8/9/2025 1:57:37 AM.

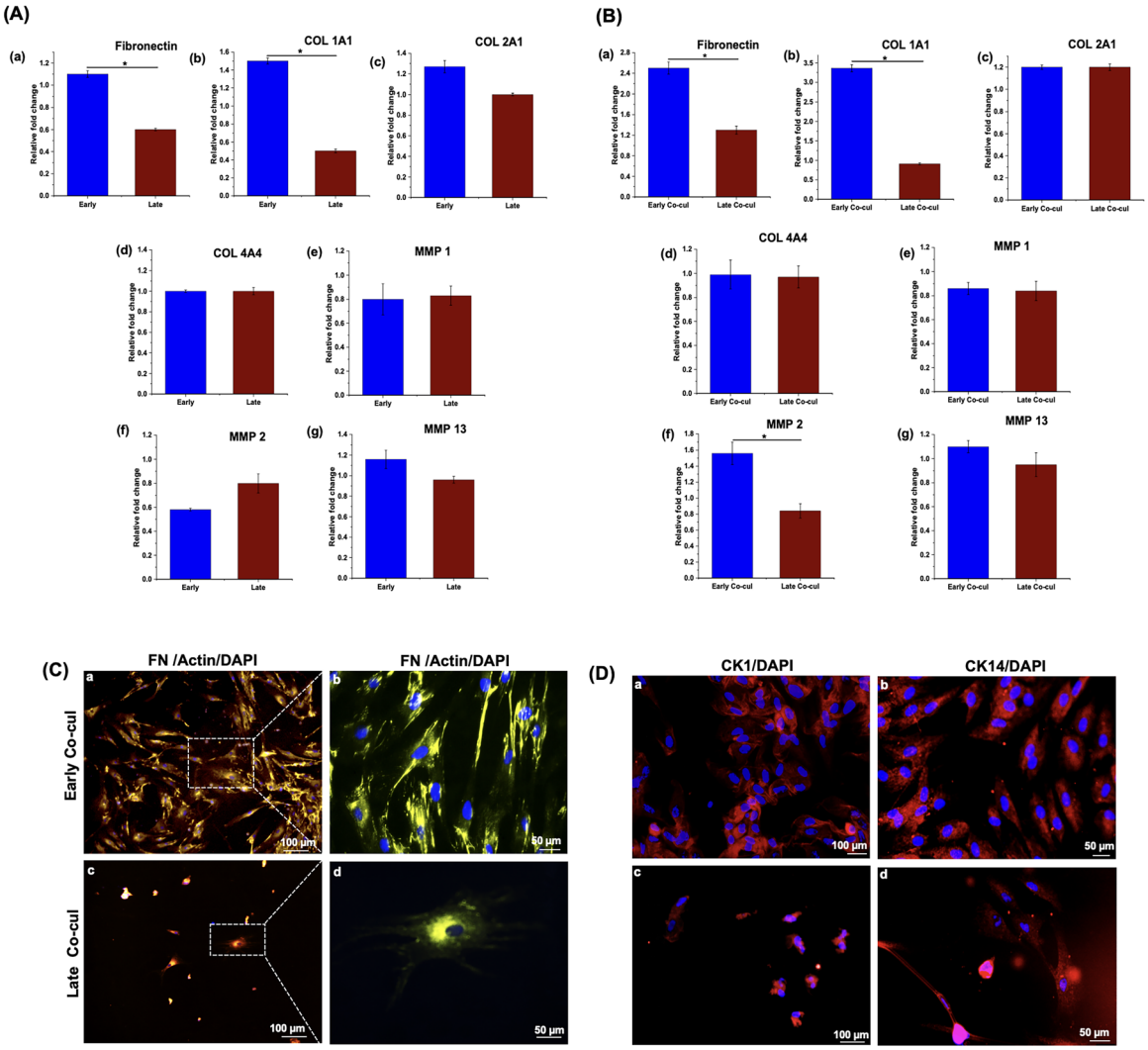


Fig. 3 Evaluation of gene expression by RT-PCR of (A) early and late passage fibroblast cells in 2D monolayer culture (a) fibronectin, (b) COL 1A1, (c) COL 2A1, (d) COL 4A4, (e) MMP-1, (f) MMP-2, and (g) MMP-13 on day 7 and (B) early and late passage fibroblast cells + keratinocytes co-culture (Co-Cul) (a) fibronectin, (b) COL 1A1, (c) COL 2A1, (d) COL 4A4, (e) MMP-1, (f) MMP-2, and (g) MMP-13 after 7 days in cornification media. Immunofluorescence analysis depicting the protein expression of (C) actin and fibronectin in (a, b) early, and (c, d) late passage (fibroblast cells in co-culture with keratinocytes after 7 days in cornification media. Fibronectin stained in green fluorescence; actin by red phalloidin. Nucleus stained blue by DAPI. (D) CK1 and CK14 were produced by differentiated keratinocytes embedded in co-culture conditions with (a, b) early and (c, d) late passage fibroblast cells in co-culture with keratinocytes after 7 days in cornification media. CK1 and CK14 were stained red, and the nucleus was stained blue by DAPI. Abbreviations: FN: fibronectin, CK: cytokeratin, Co-cul: co-culture.

passage ones. Contrastingly, a significant expression was noticed in co-culture, exhibiting a decline in the expression level in the late condition (Fig. 3B(f)). Insignificant expression was seen with the other two MMP types, *i.e.*, MMP 1 and 13, in both baselines and co-culture (Fig. 3A and B(e and g)).

**3.1.3 Protein expression of the early and late passage HDFs in co-culture.** We further ascertained the expression of actin and fibronectin along with CK1 and CK14 in the co-culture by IFC. A decreased fibronectin and actin expression was observed in the late co-culture condition after keeping them for seven days in the cornification medium (Fig. 3C(c and d)). In contrast, the expression was much higher in the early passage co-culture, which was also due to the cumulative effect of higher cell density (Fig. 3C(a and b)). This result validates our gene expression findings.

Additionally, we determined the expression of CK1 and CK14, the markers of differentiated keratinocytes. Significant differences in the expression of these proteins in the proliferative or early passage and senescent or late co-culture were obtained after seven days of differentiation in the cornification media. A decreased expression of both CK1 and CK14 was conspicuous in the late co-culture condition, with a significant reduction in the cell number (Fig. 3D(c and d)).

**3.1.4 Comparative gene and protein expression of the 3D bioprinted skin aging model.** The dermal component of the 3D bioprinted aging skin construct encapsulated with the HDF-laden in SF–G bioink was represented by the first 10 layers with a dimension of 6 mm × 25 mm (Fig. 4A(a)). The epidermal component was represented by the subsequent five layers of the

 This journal is © The Royal Society of Chemistry 2025

Published on 14 July 2025. Downloaded by Indian Institute of Technology New Delhi on 8/9/2025 1:57:37 AM.

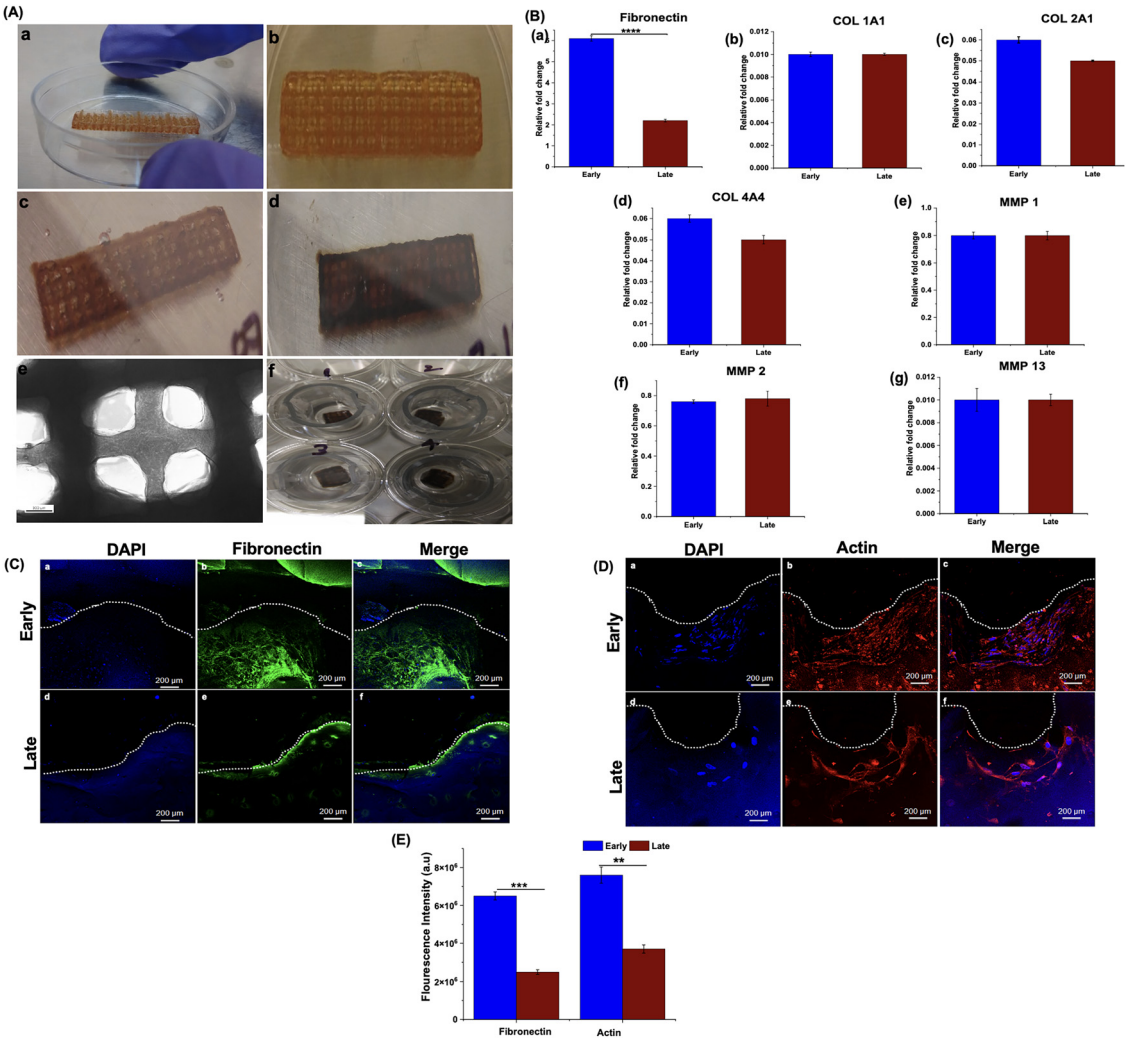


Fig. 4 (A) 3D bioprinted SF–G construct with (a) early passage fibroblast cells immediately post-bioprinting, and (b) early passage fibroblast cells kept in proliferation media for 3 days. Dual layered 6 mm × 25 mm 3D bioprinted SF–G construct with (c) early and (d) late passage fibroblast cells and keratinocytes printed as the top layer post 3 days in a 1 : 1 mixture of fibroblast and keratinocyte proliferation media, simulating the 3D skin aging model; (e) microscopic image of the 3D bioprinted construct after 3 days in a 1 : 1 mixture of fibroblast and keratinocyte proliferation media; (f) the 6 mm × 2.5 mm construct was dissected into 6 mm × 6 mm fragments and kept in Transwell culture in cornification media for 7 days. (B) Evaluation of gene expression by RT-PCR of 3D bioprinted SF–G constructs encapsulated with early and late passage fibroblast cells with keratinocytes at day 7 showing (a) fibronectin, (b) COL 1A1, (c) COL 2A1, (d) COL 4A4, (e) MMP-1, (f) MMP-2 and (g) MMP-13 expression. Immunostaining images depicting the expression of (C) fibronectin and (D) actin in 3D bioprinted SF–G constructs on day 7. (E) Fluorescence intensity comparison graphs of fibronectin and actin. Data represented as mean ± SD, significant at $p < 0.0001$. Abbreviations: SF–G – silk-fibroin–gelatin.

construct using SF–G bioink loaded with human keratinocytes, resulting in a dual-layered 3D bioprinted construct mimicking the aged skin (Fig. 4A(c and d)). The 6 mm × 25 mm dual-layered construct was then dissected into 6 mm × 6 mm small constructs and placed in an air–liquid interface in Transwell inserts for further characterization studies (Fig. 4A(f)).

Once the gene expression in baseline and co-culture was determined, we assessed the expression levels of the 3D bioprinted construct encapsulated with early/late passage HDF in co-culture with keratinocytes. A significant decrease (3.9-fold) in the expression of fibronectin was observed in the 3D bioprinted construct with the late passage, supporting the results obtained in the baseline expression and co-culture (Fig. 4B(a)). Although a nominal decrease in the fold change was observed with COL 2A1 and COL 4A4 in the late passage (Fig. 4B(c and d)), overall, no change in MMPs and collagen isoforms was observed in the 3D bioprinted construct (Fig. 4B(e, f and g)).

Determination of the actin and fibronectin expression in the 3D bioprinted construct with early/late passage HDFs in co-culture is essential to validate whether our 3D bioprinted skin aging construct mimics the aging conditions in the native skin. A decreased expression of ECM protein fibronectin and actin in late passage fibroblast cells in the 3D bioprinted construct was observed (Fig. 4C and D), which validates the gene expression findings. More cells were found to be present in the early passage constructs, as evident from DAPI staining (Fig. 4C(a) and D(a)). Hence, an apparent morphological change in the early and late passage HDFs in co-culture was observed in the 3D bioprinted construct mimicking the aged skin.

Published on 14 July 2025. Downloaded by Indian Institute of Technology New Delhi on 8/9/2025 1:57:37 AM.

**3.1.5 Analysis of differential protein expression by MALDI-TOF and STRING analysis.** The differential expression profiles of the proteins obtained in MALDI-TOF from their selected bands (Band 1–12) *via* SDS-PAGE analysis (Fig. 5A) with their molecular functions mentioned in Table 2. We obtained several proteins expressed in 2D and co-culture related to cell differentiation and proliferation. Cilia- and flagella-associated protein 53 and actin-related protein 2/3 complex subunit 3 were identified only in the 3D bioprinted early passage skin aging construct. Our cumulative data suggest that this approach might be helpful for chronological skin aging.

An extensive degree of gene networking was discovered by gene ontological analysis by STRING among the genes investigated during the development of aged skin (Fig. 5B). We noticed gene ontology biological processes related to skin morphogenesis, endodermal cell differentiation, collagen metabolic process, ECM disassembly, cell–substrate junction assembly, cell adhesion mediated by integrin, collagen fibril organization, wound healing, *etc.* Furthermore, the KEGG pathway related to our genes in the study was linked to ECM receptor interaction, the AGE-RAGE signaling pathway in diabetic complications, and the Relaxin signaling pathway (Fig. 5C).

## 3.2 Aging induced by $H_2O_2$ and high glucose

**3.2.1 Features of the $H_2O_2$ and high glucose-treated HDFs.** Upon treatment of the early passage HDFs with $H_2O_2$, a clear differentiated morphology of the normal (untreated) *versus* the $H_2O_2$-treated cells was observed on day 7, as shown in Fig. 6A(a

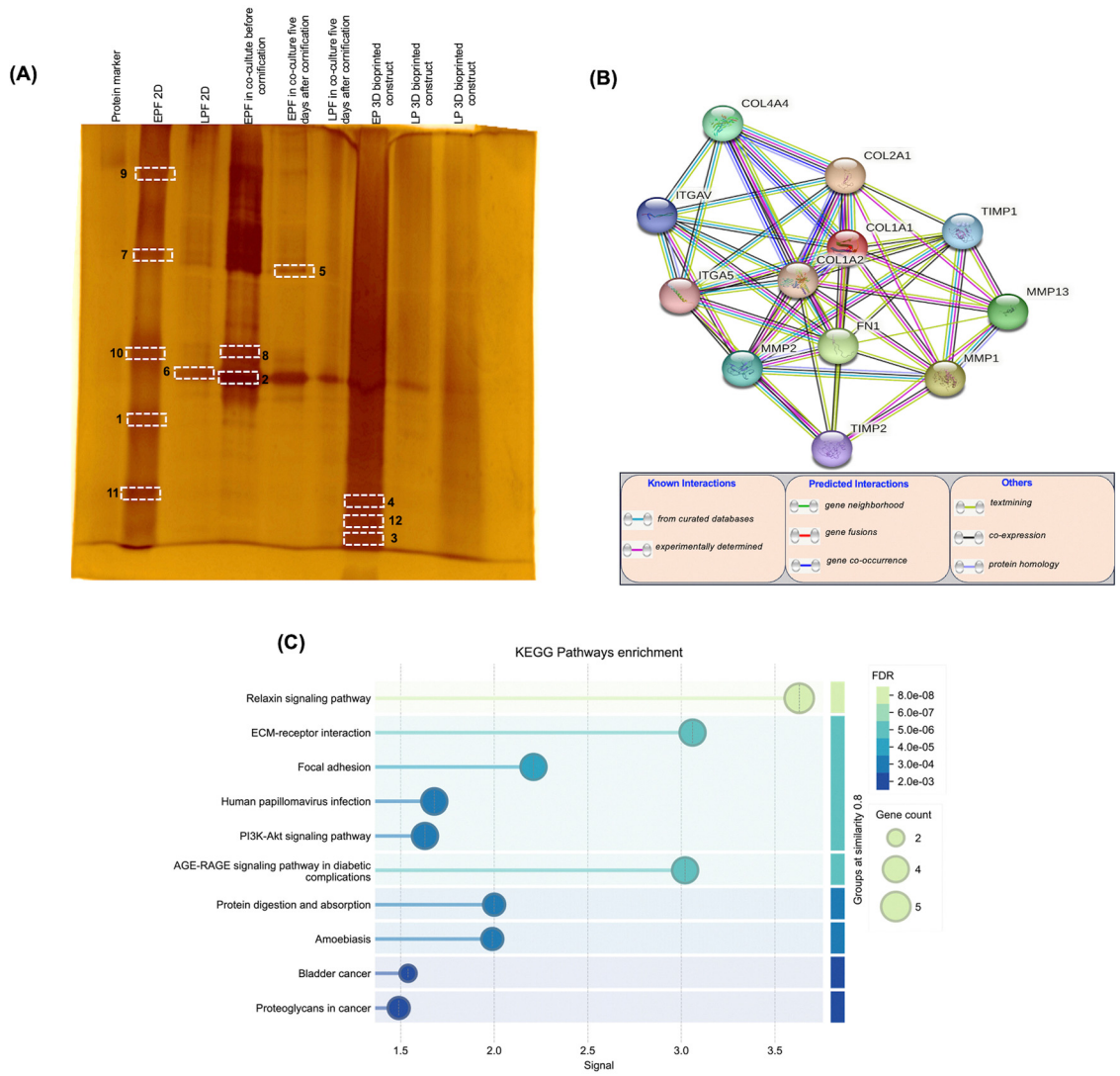


Fig. 5 (A) Protein expression profile of early and late HDFs in 2D (lane 2 & 3), co-culture (early passage fibroblasts before cornification, lane 4), and lanes 5 & 6 represent the early/late passage HDFs in co-culture with keratinocytes after 7 days in cornification media, lane 7 early passage 3D bioprinted SF–G construct after 7 days in Transwell, lane 8 & 9 late passage 3D bioprinted SF–G construct after 7 days in Transwell. Highlighted red box showing differentiated protein bands, which are identified by MALDI-TOF. (B) STRING protein–protein expression of the proteins in the SF–G bioprinted construct. (C) Visualization of the KEGG pathway enrichment analysis of the differentially expressed genes in the SF–G bioprinted construct. Abbreviations: EPF – early passage fibroblast, LPF – late passage fibroblast, LP – late passage.

 This journal is © The Royal Society of Chemistry 2025

Published on 14 July 2025. Downloaded by Indian Institute of Technology New Delhi on 8/9/2025 1:57:37 AM.

Table 2 Illustration of the bands identified in MALDI-TOF and their molecular function

| Band ID | Symbol | Name | Molecular weight (approx. kDa) | Mascot score | No. of peptide matched | Function |
|---|---|---|---|---|---|---|
| 1 | MYH1 | Myosin-1 | 45 | 157 | 21 | Plays key role in age-related changes in muscle contractility. Propels actin filament that impacts aging |
| 2 | PTPC-1 | Protein tyrosine phosphatase domain-containing protein 1 | 56 | 230 | 15 | Signaling molecules that regulate a variety of cellular processes including cell growth, differentiation, mitosis, and oncogenic transformation |
| 3 | OCLM | Oculomedin | 5.3 | 293 | 11 | The function is not completely understood, generally expressed in trabecular cells and retina following mechanical stretching |
| 4 | MB21D2 | Protein Mab-21 domain containing 2 (human) | 38 | 93 | 10 | Uncharacterized protein C3orf59; mab-21 domain-containing protein 2, Go – molecular function shows cadherin binding |
| 5 | RHOBTB1 | Rho-related BTB domain containing 1 | 79 | 235 | 23 | Key regulators of the actin filament system and, consequently, of all processes that depend on the reorganization of the actin cytoskeleton, such as membrane trafficking, cell motility, cytokinesis, adhesion, and morphogenesis. They have also been implicated in numerous processes not directly linked to actin reorganization, like NADPH oxidase activation, microtubule organization, gene expression, cell cycle progression, apoptosis, and tumorigenesis |
| 6 | UCHL1 | Ubiquitin carboxyl-terminal hydrolase 17-like protein | 59 | 355 | 13 | Deubiquitinating enzyme that removes conjugated ubiquitin from specific proteins to regulate different cellular processes that may include cell proliferation, progression through the cell cycle, apoptosis, cell migration, and the cellular response to viral infection |
| 7 | ZNF569 | Zinc finger protein 569 | 79.5 | 437 | 20 | Involved in transcriptional regulation |
| 8 | hnRNP M | Heterogeneous nuclear ribonucleoprotein M isoform X6 | 68 | 79 | 15 | May initiate a series of signaling events leading to tyrosine phosphorylation of proteins and induction of IL-1 alpha, IL-6, IL-10, and tumor necrosis factor-alpha cytokines |
| 9 | ADCY8 | Adenylate cyclase type 8 | 140 | 619 | 21 | Plays an important role in aging |
| 10 | CFAP53 | Cilia- and flagella-associated protein 53 | 61 | 120 | 13 | Expressed by the ciliated cells of the frog epidermis and in skin fibroblasts from humans. May play a role in the beating of primary cilia and thereby be involved in the establishment of organ laterality during embryogenesis |
| 11 | ARPC3 | Actin-related protein 2/3 complex subunit 3 | 40 | 102 | 14 | Functions as a component of the Arp2/3 complex which is involved in the regulation of actin polymerization and together with an activating nucleation-promoting factor (NPF) mediates the formation of branched actin networks |
| 12 | ELOC | Elongin-C | 15 | 128 | 11 | Involved in the aging regulatory pathway |

and b). In response to the $H_2O_2$ treatment, there was an augmentation in the cell volume and surface irregularity, and cells were observed to be adherent. Mild cytotoxicity was observed on day 1 (data not shown) as apoptotic bodies in culture media; however, the fibroblast cells recovered their proliferative capacity on day 7 (Fig. 6A(b)) due to the exposure to $H_2O_2$ for a short period of 120 min. When treated with SA-β-Gal, the $H_2O_2$-treated fibroblast cells exhibited a high activity of β-Gal-positive staining, which signifies an elevated rate of the occurrence of senescence compared to the control cells (Fig. 6A(c and d)). Hence, a significant induction was observed on day 7 ($p < 0.01$).

Further confluent young HDFs were treated with high glucose to imitate diabetic conditions. An increase in cell density was observed when cultured in the proliferation media. Morphologically, they appeared more elongated and spindle-shaped (Fig. 6B(a)). Culturing the fibroblasts in high glucose medium not only resulted in a decrease in the cell number but also demonstrated stagnant growth (senescence) morphology and declined replicative life span (Fig. 6B(b)). Under high glucose conditions, the HDF exhibited a high percentage of SA-β-Gal positive staining, which signifies an elevated rate of senescence compared to the control. Therefore, a significant induction of β-gal activity was reported under high glucose compared to the control (Fig. 6B(d)).

Although a decrease in the telomere length was observed in $H_2O_2$-treated fibroblasts at day 7, no significant induction of telomere length shortening was observed on day 14 (Fig. 6C). In contrast, in the presence of high glucose, the young fibroblast cells showed a progressive reduction in the telomere length during prolonged culture time at day 7 and 14, respectively, compared to that observed on day 3 (Fig. 6D).

**3.2.2 DNA damage study.** The DNA damage is measured as an indication of genotoxicity and is accomplished by specific antibody-based detection of phosphorylated H2AX (Ser139) in the nucleus. Cytotoxicity is measured with the Image-iT® DEAD Green™ viability stain. The Image-iT® DEAD Green™ viability stain has a high affinity for DNA, is non-fluorescent, and impermeant but forms highly fluorescent and stable dye-nucleic acid complexes when bound to DNA. Staining of nuclear DNA cannot occur in live cells due to the impermeability of the plasma membrane for the stain. This property enables the discrimination of dead cells with Image-iT® DEAD Green™ viability stain. Hoechst 33342 dye stains nuclear DNA in live and dead cells.

$H_2O_2$ is a strong oxidant that is toxic to cells. To quantify $H_2O_2$-induced DNA damage, immunolabelling was conducted

Published on 14 July 2025. Downloaded by Indian Institute of Technology New Delhi on 8/9/2025 1:57:37 AM.

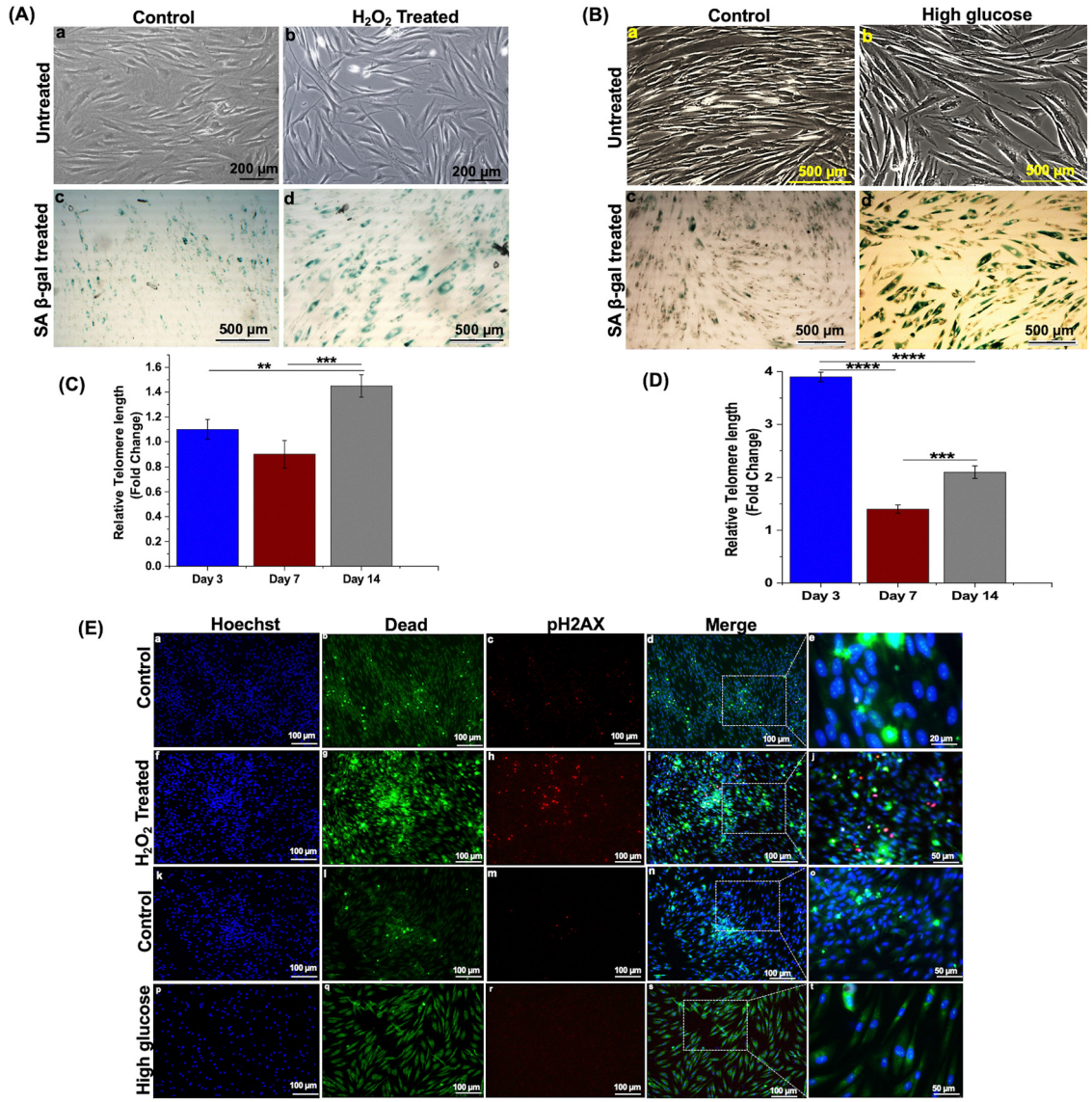


Fig. 6 Bright field microscopic images depicting the morphology of (A) (a) and (b) control and $H_2O_2$ treated fibroblast cells (P-6) before; and (c) and (d) after staining with senescence-associated (SA) β-galactosidase on day 7; (B) (a) and (b) control and high glucose treated fibroblast cells (P-6) before; and (c) and (d) after staining with senescence-associated (SA) β-galactosidase on day 7. (C) and (D) Quantification of the relative telomere length of the $H_2O_2$ and high glucose-treated fibroblast cells on days 3, 7, and 14, respectively. (E) Immunofluorescence analysis of HCS DNA damage staining of fibroblast cells (P-6) (a)–(e) control; (f)–(j) treated with 200 μm $H_2O_2$ on day 7; (k)–(o) cultured in proliferation media at day 7; (p)–(t) cultured in high glucose medium on day 7.

on day 7 after exposure to 200 μM $H_2O_2$. Our results indicated that $H_2O_2$-induced DNA damage became statistically significant ($p < 0.05$) on day 7. A substantial increase in dead cell populations occurred, and $H_2O_2$ significantly increases acute cell death in cultured fibroblasts in a time-dependent manner (Fig. 6E(i and j)).

The induction of pH2AX, a sensitive marker of DNA damage, was also determined in fibroblast cells treated with a high glucose concentration (50 mM). Notably, from the obtained IFC study, it was evident that the fibroblast cells didn't undergo any Hoechst damage in the presence of 50 mM glucose (Fig. 6E(s and t)). This was validated by innumerable nuclei, which were evident from DAPI staining. Compared to the control, a drastic reduction in the dead cells and DNA damage was evident upon treatment with high glucose.

**3.2.3 Comparative gene expression analysis.** To gain insight into the effect of exposure to 200 μM $H_2O_2$ and high glucose on HDFs, extensive gene expression analysis was carried out on days 3, 7, and 14. The highest fibronectin expression was 4 fold on day 7, which decreased on day 14 but was around 2-fold higher than the control (Fig. 7A(a)). On the other hand, the highest level of fibronectin expression upon glucose treatment was observed on day 14 (Fig. 7B(a)). Under both conditions, there was an insignificant change in the expression of COL 1A1 (Fig. 7A and B(b)). COL 2A1 demonstrated a 2-fold increase in expression on day 14 compared to the control;

 This journal is © The Royal Society of Chemistry 2025

Published on 14 July 2025. Downloaded by Indian Institute of Technology New Delhi on 8/9/2025 1:57:37 AM.

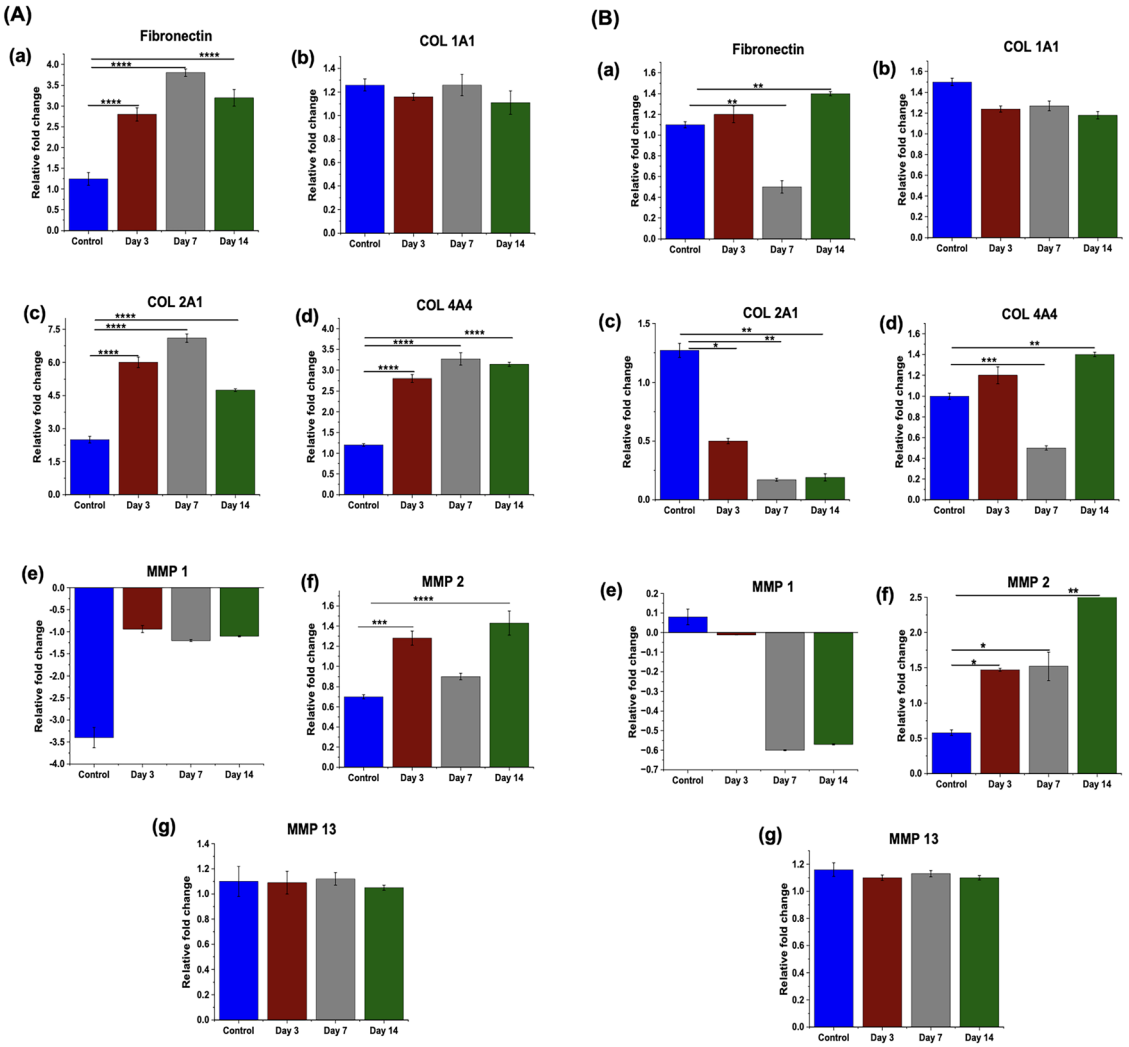


Fig. 7 Evaluation of gene expression by RT-PCR of (A) $H_2O_2$ and (B) high glucose treated fibroblast cells showing (a) fibronectin, (b) COL 1A1, (c) COL 2A1, (d) COL 4A4, (e) MMP 1, (f) MMP 2 and (g) MMP 13 expression on day 3, 7 and 14.

however, a 3-fold decrease in the expression was observed on day 7 (Fig. 7A(c)). Interestingly, although under high glucose-treated conditions the expression on day 14 was less than that on day 3, and the fold change was less than one (Fig. 7B(c)). With COL 4A4, an increase in the expression level was observed under both conditions on day 14 compared to that on day 3 (Fig. 7A and B(d)). An interesting observation was noticed with MMP 1 under both conditions. In both instances, a negative fold change was exhibited (Fig. 7A and B(e)). With MMP 2, an increased expression was observed on day 14 compared to other time points (Fig. 7A and B(f)). However, MMP 13 showed no significant difference in expression profile upon $H_2O_2$ and high glucose treatment (Fig. 7A and B(g)).

**3.2.4 Cell cycle analysis.** Cell cycle analysis revealed three distinct cell populations in cultured fibroblast cells treated with 200 μM $H_2O_2$, which were indicative of cells in the $G_0/G_1$, S, and $G_2/M$ phases of the cell cycle (Fig. 8A and B). The untreated (control) showed greater accumulation of cells in $G_0/G_1$ (85.6% ± 2.9%), S (4.05% ± 0.9%), and $G_2/M$ (8.06 ± 0.8%). After exposure to 200 μM of $H_2O_2$, there was a significant decrease in the cell population in the S phase ($p < 0.01$), whereas after 72 h the percentage of cells were control = 4.05%, 24 h = 3.8%, 48 h = 3.03% and 72 h = 0.66% (Fig. 8A). Interestingly, day 7 showed no change in the distribution of the cells in the cell cycle after treatment (data not shown). Achieving a prolonged G arrest by $H_2O_2$ might necessitate the cells to be in the phase before G, before treatment.

Similarly, the distribution of the fibroblast cells treated with 50 mM glucose showed that the synthetic or the 'S' phase was progressively reduced after 48 and 72 h, respectively. In contrast, the number of cells in the G1 phase increased from 24 to 48 h compared to the control (Fig. 8C and D).

## 4. Discussion

Skin aging and cosmetic research are specifically prone to concerns associated with animal testing. Apart from the ban

Published on 14 July 2025. Downloaded by Indian Institute of Technology New Delhi on 8/9/2025 1:57:37 AM.

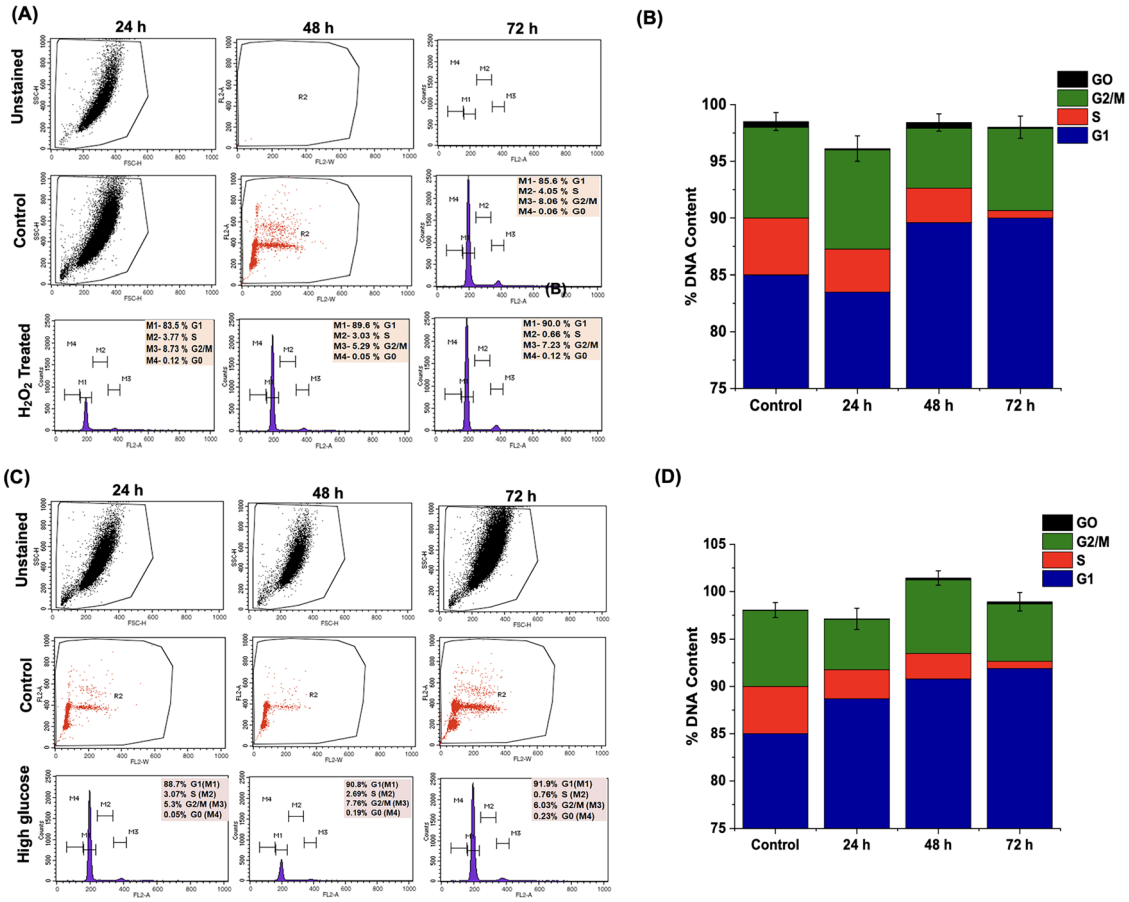


Fig. 8 Cell cycle analysis by propidium iodide (PI) staining using flow cytometry. Cultured fibroblast cells were treated with (A) 200 μM $H_2O_2$ and analysed at 24, 48, and 72 h after exposure, and (B) cell cycle analysis calculated as $G_1$, S phase, and $G_2$M from the histogram of the flow cytometry analysis. (C) 50 mM of high glucose and analysed at 24, 48, and 72 h. (D) Cell cycle analysis was calculated as G1, S phase, and G2M from the histogram of the flow cytometry analysis.

by the European Union on animal testing, scientific and economic rationale have compelled researchers to look for alternative *in vitro*-based models[50] Besides, the existing tissue-engineered aged skin equivalents fail to imitate the DEJ, which is corrugated to form the rete-ridges. In addition to allowing researchers to examine the impact of DEJ on cell activity, the emergent ability to fabricate ever-more-complex constructs for skin TE will facilitate the creation of morphological and physiological mimics that are more similar to actual aged skin.[51] An ideal 3D-based model for skin aging that can adequately mimic the intricate microenvironment of the native tissue is yet to be developed. To the best of our knowledge, this is the first study demonstrating the spatial organization of co-cultured dermal fibroblasts and keratinocytes of human origin utilizing SF–G bioink. This provides a feasible approach for establishing an *in vitro* skin aging model replicating the microenvironment of native human-aged skin. We focused on two conditions: (a) the development of a dual-layered 3D bioprinted skin aging model and (b) the use of $H_2O_2$ and high glucose as aging-inducing agents, which mimic the oxidative stress and diabetic condition, one of the primary reasons for skin aging.

We started with the baseline experiments with early and late passage HDF. The alteration in morphology in the late passage is considered a unique feature of senescent fibroblasts.[52] Although very little is known regarding these changes in the senescent stage, most senescence-based mechanistic studies have concentrated on irreversible growth arrest.[53] From the morphological characteristics, we deduced that, even though late passage cells have ceased replication, they remain enlarged, which necessitates evaluating whether cell enlargement and growth arrest share the same control process. Conventionally, senescent cells arise from cell replication such that most HDF strains from fetal tissue undergo 50–60 population doublings before senescence.[54] Senescent cells have a broader and flatter body than healthy cells, which are spaced out. These modifications could be attributed to cell-cycle arrest in the G1/G2 phase following generation. Furthermore, they are determined by large nuclei, presumably due to the loss of lamin B1 from the inner surface of the nuclear envelope. Interestingly, these senescent fibroblast cells were observed to take a longer time to detach during trypsinization than the proliferative ones. SA-β-gal, one of the widely used markers, was used to ascertain the senescent cells both *in vitro* and *in vivo*, detectable at suboptimal pH 6.0.[55] It is found that the number and size of lysosomes increase in late passage cells; hence, the enhanced

 This journal is © The Royal Society of Chemistry 2025

Published on 14 July 2025. Downloaded by Indian Institute of Technology New Delhi on 8/9/2025 1:57:37 AM.

activity of SA-β-gal in senescent fibroblasts occurs at least in part due to the surge in lysosomal β-gal levels.[56] Apart from the SA-β-gal staining, a decrease in the telomere length in the late passage fibroblasts established the distinguishing features of the passage-dependent cells. Fibronectin, a secreted matrix protein, is a bridge between the ECM substrate and cell surface integrins, which is structured as a mesh of fibrils, much like collagen. Decreased expression in the late passage fibroblasts implies that impaired (anisotropic) structural arrangement of fibronectin fibers, together with decreased fibronectin synthesis, are both signs of cellular aging.[57]

The majority of *in vitro* aging research relies on fibroblast cell culture.[16] In healthy skin, keratinocytes, which constitute 95% of the epidermis, actively interact with fibroblasts to help maintain the skin's homeostasis.[58,59] Little focus has been placed on the role of keratinocytes for their potential to contribute to skin aging.[58] Numerous studies prove that epithelial–dermal interactions are significant; for instance, soluble substances secreted by fibroblasts influence epidermal development, and glycation of the dermis was found to modify integrin expression in the epidermis.[60] Additionally, it has been demonstrated that keratinocytes regulate fibroblasts' manufacture of elastin and that fibroblasts influence keratinocyte differentiation. Hence, this study focused on considering the interplay between the fibroblast and keratinocytes in co-culture. The two main ECM components that fibroblasts produce are fibronectin and COL 1A1, the hallmark of the functional dermis.[61] A decreased gene expression both in baseline and co-culture implies deleterious effects on the function and maintenance of the dermal layer, contributing to aging.[62] The decline in the expression of the collagen isoforms could be corroborated by the fact that fibroblasts' attachment is impeded in aged skin due to the continuous degradation of the ECM, which is mainly composed of collagen type I[63,64] and collagen IV, on the other hand, it comprises the basic ultrastructure of the basement membrane of the skin.[65] Contrastingly, the fibroblast remains attached to the surrounding intact ECM in its young counterparts.[64,66] MMPs, the essential enzyme involved in the degradation of all dermal ECM proteins and cutaneous photo-aging, exhibited a contrasting trend; the expression level was highly insignificant both in baseline and co-culture. This decrease in fibronectin expression in late co-culture was further validated by IFC analysis, which was also accompanied by a decline in actin expression. Furthermore, the expression of the basal epidermal marker CK14 (Stratum basale) *via* IFC, indicative of proliferating keratinocytes, had reduced in the late co-culture, akin to that observed in human aged skin.[67] Additionally, the expression of CK1 in the early co-culture, a hallmark of keratinocyte differentiation and stratification[68] implied signified maturation and terminal differentiation of the keratinocytes, which is involved in developing a cornified epidermal layer. However, decreased expression in late co-culture signifies loss of cellular integrity, leading to intrinsic skin aging.[67]

Fibroblasts encapsulated in SF–G were initially solely printed as the dermal layer, allowed to proliferate for three days, followed by the printing of the top epidermal layer with keratinocytes, which mimics the DEJ of the native human skin. This dual-layered bioprinted construct represents the human-aged skin model. This was validated by reduced fibronectin/actin gene and protein expression in the constructs with the late passage cells in co-culture. It must be noted that morphological properties like cell area, spreading, focal adhesion, *etc.*, are controlled by the mechanical features of the environment surrounding the ECM.[69–71] Notably, the variation in cellular morphology is governed by the actin filament assembly that produces protrusions and contractile stress fibers. Alteration in the expression in the senescent cells might be a vital feature of a generalized decline in cellular functioning related to aging.[72] Furthermore, alteration in the actin cytoskeleton and direct impact on the arrangement of the ECM could result in an alteration in the gene expression in senescent fibroblasts, resulting in a decline in the ECM protein synthesis.[73] Our results also confirm the actin network's key role concerning the cells' mechanical characteristics, suggesting that the extent of actin polymerization in senescent fibroblasts is transferred into filamentous form. This advocates that the age-associated decline in cell flexibility is embedded in modified polymerization of the actin cytoskeleton.[73]

Aging in humans is advocated by the interplay of a series of proteins. We identified the expression of such proteins in our bioprinted construct by MALDI-TOF analysis, as mentioned in Table 2. For example, the presence of MYH1 protein provides evidence of age-related fibrotic risk.[74] CFAP53, commonly known as the cilia and flagella-associated protein 53, although it does not directly control aging, it may indirectly affect age-related processes by influencing tissue homeostasis and repair through its role in cilia function and cell division.[75] Adenylyl cyclase 8, which is encoded by the ADCY8 gene, contributes to aging, especially with respect to cardiac aging and related inflammation.[76] Apart from that, the presence of PTPC-1[77] and ELOC,[78] plays a significant role in the aging process. For example, mutations in ELOC may modify cellular responses to hypoxia and shorten longevity by interfering with the ubiquitination-mediated clearance of HIF-1. Furthermore, the KEGG pathway analysis corroborates these findings, highlighting the involvement of ECM–receptor interaction and the AGE–RAGE signaling pathway that contributes significantly to aging and illnesses associated with aging. The skin's ECM, which supports structure and controls cell activity, deteriorates with age. Cell–ECM interactions are disrupted by this degradation and changes in cell-surface receptors like integrins, which impair skin function and contribute to aging symptoms, including wrinkles and decreased suppleness.[79] With age, AGEs, which are created by the non-enzymatic glycation of proteins and lipids, build up and can attach to RAGE, initiating signaling cascades that lead to tissue damage and cellular malfunction.[80] Numerous cross-links found in collagen have been identified, and their correlation with vascular disease has highlighted the significance of AGEs in both aging and diabetes problems.[80] RAGE-dependent inflammation in the macro- and microvasculature plays a role in the pathophysiology of diabetes. Research on the relaxin signaling pathway, specifically the roles of the neuropeptide relaxin 3 receptor, *i.e.*, RXFP3, has

Published on 14 July 2025. Downloaded by Indian Institute of Technology New Delhi on 8/9/2025 1:57:37 AM.

revealed that RXFP3 may be essential for several aging-related conditions because it has been linked to a number of aging markers, including oxidative stress and the DNA damage response.[81] It is noteworthy that the KEGG pathway enrichment analysis of our differentially expressed genes in the 3D bioprinted model revealed the engagement of the pathways related to the relaxin signaling pathway, ECM–receptor interaction, and the AGE–RAGE signaling pathways in diabetes complications, all of which play a crucial role in aging. One factor to which utmost attention must be given is that after many passages, cells started losing their proliferative capacity and metabolic activity (late passages), resulting in a low cell density. As a result, we needed to optimize the number of cells required for 3D bioprinting. Taken together, our 3D bioprinted model can simulate the aging skin *in vitro* and be used as a screening platform for drugs and cosmetic testing.

As a more rapid alternative to using replicative senescent fibroblasts, we induced senescence prematurely using $H_2O_2$, which acts as an oxidative stress, and by using high glucose, which mimics the diabetic condition, which is another major factor contributing to aging. Recent studies suggest that in the presence of oxidants, early passage fibroblasts can phenotypically resemble the senescent ones.[35,82] An exposure of 400 or 500 μM concentration of $H_2O_2$ has been reported to be cytotoxic to the cultured fibroblast cells.[83] Therefore, in our study, we have optimized a concentration of 200 μM of $H_2O_2$, which is suitable for inducing senescence, as shown previously by Chen and Ames.[35] Compared to the control, enhanced β-gal activity in the treated proliferative fibroblast suggests that a mere 120 min exposure is sufficient to induce senescence. This further dismisses the need for prolonged exposure, which was mentioned earlier by several other studies.[36] In a similar study, Jin *et al.* treated human diploid fibroblasts with 60% glucose restriction or high glucose medium.[84] They reported a decrease in cell growth and an increase in apoptosis with high glucose concentration, similar to our results. 50 mM glucose concentration was chosen for our study since fibroblasts can grow favorably at a concentration of 10–20 mM. However, a concentration above 50 mM was reported to have an impeding proliferative effect, and more than that was found to be cytotoxic.[85] Although studies[86,87] depict that high glucose concentration impedes fibroblast proliferation, the mechanisms involved in glucose-promoting senescence are still not precisely understood. Therefore, in the present study, we probed into the effect of aging by incubating HDFs with high glucose concentration (imitating diabetic conditions). SA-β-gal staining in both cases confirmed aging induction by $H_2O_2$ and high glucose conditions. Although a shortening in telomere length was observed on day 7 compared to day 3 with high glucose, it did shorten in the presence of $H_2O_2$. DNA damage, such as single-strand DNA breaks, may result from exposure to free radicals or oxidants; hence, the telomere shortening rate is assumed to be partly dependent on intracellular oxidative stress.[88] Treatment with $H_2O_2$ for 120 min in our study might be a probable reason for the non-significant shortening of telomere length on day 7 compared to day 3. On the other hand, Duan *et al.* reported that HDFs, when treated with low doses of $H_2O_2$ for a long time, gave rise to irreversible cellular senescence, increasing the rate of telomere shortening.[36] This indicates no effect of $H_2O_2$ at doses ranging from 50 to 200 μM on telomere shortening. These results suggest that $H_2O_2$ might not be involved directly in shortening telomeres. It is worth noting that although we have not detected the ROS expression under both conditions, the elevated levels of MMP-1 direct the presence of ROS, one of the causative agents of ageing. ROS can directly activate the enzyme through oxidative stress or indirectly affect MMP-1 activity and expression by altering signaling networks contributing to its transcription. Hence, the gene expression analysis and DNA damage study illustrate the potency of both agents in inducing aging.

Growth arrest is a critical feature of senescent cells, and the percentage of cells present in the $G_0/G_1$ phase is a definitive index for evaluating proliferative activity.[89] A histogram plot of DNA content against cell numbers gives the classical DNA profile for a proliferating cell culture. Leonardo[90] *et al.* exhibited that cells in the early to middle $G_1$ phase undergo an elongated growth arrest following γ-irradiation. Whereas, cells when treated in the late $G_1$ phase invaded the S phase, followed by their entry into the $G_2$ phase when treated in the S phase, and arrested before mitosis.[91] The sub-lethal concentration of $H_2O_2$ used by us induced senescence-like growth arrest in the HDFs, unlike the cells that experienced necrosis or apoptosis due to the cytotoxic concentration of $H_2O_2$.[48,92] Apoptosis is a principal phenotype detected in cells treated with $H_2O_2$ concentrations of around 300–400 μM, in contrast, both the senescence and apoptosis-like phenotypes are observed in cells treated with 200 μM $H_2O_2$.[93] It should be noted that although we have achieved senescence-like characteristics with 200 μM $H_2O_2$, however, we did not use any marker for apoptosis in this study which makes it difficult to determine whether the HDF underwent apoptosis or not. A decrease in the cell population in the 'S' phase of the cell cycle under glucose conditions indicates the loss of DNA repair and synthesis, a marker of aging. An increase in HDF concentration in the G0/G1 phase indicates that high glucose impeded the $G_1$–S transition compared to the control. This finding was as per the results obtained by Li *et al.*,[89] where they dictated the regenerative and protective outcome of calcium silicate on fibroblasts treated with high glucose. Hence, the results obtained with $H_2O_2$ and high glucose support using these agents as an alternative approach in developing a 3D bioprinted skin aging model dictate its suitability for new drug targets. However, from the results obtained, we can conclude that high glucose conditions could mimic the aging characteristics to a greater extent than that of the $H_2O_2$.

## 5. Conclusion

We developed a 3D bioprinted skin aging model employing SF–G. Through this study, we illustrated for the first time (i) the extrusion-based 3D bioprinting approach helped mimic the dual-layered of the aged skin by allowing the spatial distribution of HDF and human epidermal keratinocytes, (ii) recapitulated the

 This journal is © The Royal Society of Chemistry 2025

Published on 14 July 2025. Downloaded by Indian Institute of Technology New Delhi on 8/9/2025 1:57:37 AM.

dermal–epidermal junction, not possible in monolayer based models, (iii) gene and protein expression with dermal and epidermal specific markers, indicating the absolute stratification of the developed model, (iv) established the use of $H_2O_2$ and high glucose as potential senescence inducing agents, that can provide an alternative approach for the development of 3D bioprinted models. Although both $H_2O_2$ and high glucose showed high potential in inducing senescence, high glucose could mimic the aging conditions more effectively.

Our developed model can serve as a screening platform for anti-aging drugs and cosmetics. Furthermore, it can ascertain the relative contribution of various molecular mechanisms to the skin aging phenotype. Additionally, senescent cell integration in aged skin models makes them a good testing ground for senolytics and research to develop agents to delay, prevent, alleviate, or reverse age-related diseases.

## Author contributions

JC: conceptualization, methodology, investigation, writing – original draft, data curation, preparation of data, and writing – review & editing. AG: methodology, investigation, and formal analysis. SG: conceptualization, resources, supervision, funding acquisition, validation, and writing – review & editing.

## Conflicts of interest

The authors declare no conflicts of interest.

## Note added after publication

This article replaces the version published on 14 July 2025, which contained an error in the sub-heading of Section 2.12 that has since been corrected.

## Data availability

All the necessary data have been provided in the main text. Any additional data related to this paper can be obtained from the corresponding author upon reasonable request. This study did not generate/analyse datasets or code.

## Acknowledgements

JC is grateful to the Indian Council of Medical Research (ICMR), India for the Senior Research Fellowship (ICMR-SRF), File no. 5/3/8/36/ITR-F/2022-1TR.

## References

1 C. López-Otín, M. A. Blasco, L. Partridge, M. Serrano and G. Kroemer, *Cell*, 2013, **153**(6), 1194–1217.
2 Q. M. Chen, K. R. Prowse, V. C. Tu, S. Purdom and M. H. K. Linskens, *Exp. Cell Res.*, 2001, **265**, 294–303.
3 H. Chen, Y. Li and T. O. Tollefsbol, *Mol. Biotechnol.*, 2009, **41**(2), 194–199.
4 J. L. Hu, M. E. Todhunter, M. A. LaBarge and Z. J. Gartner, *J. Cell Biol.*, 2018, **217**(1), 39–50.
5 M. V. M. Milioli, H. Burger, R. Olivieri, M. Michels, P. Ávila, M. Abatti, A. Indalécio, C. Ritter and F. Dal-Pizzol, *Neurosci. Lett.*, 2019, **708**, 134339.
6 U. Herbig, M. Ferreira, L. Condel, D. Carey and J. M. Sedivy, *Science*, 2006, **311**(5765), 1257.
7 M. Tosato, V. Zamboni, A. Ferrini and M. Cesari, *Clin. Interventions Aging*, 2007, **2**(3), 401–412.
8 R. Weinmüllner, B. Zbiral, A. Becirovic, E. M. Stelzer, F. Nagelreiter, M. Schosserer, I. Lämmermann, L. Liendl, M. Lang, L. Terlecki-Zaniewicz, O. Andriotis, M. Mildner, B. Golabi, P. Waidhofer-Söllner, K. Schedle, G. Emsenhuber, P. J. Thurner, E. Tschachler, F. Gruber and J. Grillari, *npj Aging Mech. Dis.*, 2020, **6**, 1–7.
9 D. Triglia, S. S. Braa, C. Yonan and G. K. Naughton, *In Vitro Cell. Dev. Biol.: Anim.*, 1991, **27**, 239–244.
10 S. R. Slivka, L. K. Landeen, F. Zeigler, M. P. Zimber and R. L. Bartel, *J. Invest. Dermatol.*, 1993, **100**, 40.
11 K. R. Mewes, M. Raus, A. Bernd, N. N. Zöller, A. Sättler and R. Graf, *Skin Pharmacol. Physiol.*, 2007, **20**(2), 85–95.
12 M. Bataillon, D. Lelièvre, A. Chapuis, F. Thillou, J. B. Autourde, S. Durand, N. Boyera, A. S. Rigaudeau, I. Besné and C. Pellevoisin, *Int. J. Mol. Sci.*, 2019, **20**(9), 2240.
13 M. Bataillon, D. Lelièvre, A. Chapuis, F. Thillou, J. B. Autourde, S. Durand, N. Boyera, A.-S. Rigaudeau, I. Besné and C. Pellevoisin, *Int. J. Mol. Sci.*, 2019, **20**, 2240.
14 J. C. Lago and M. B. Puzzi, *PLoS One*, 2019, **14**(7), e0219165.
15 M. Dos Santos, E. Metral, A. Boher, P. Rousselle, A. Thepot and O. Damour, *Matrix Biol.*, 2015, **47**, 85–97.
16 L. Costello, T. Dicolandrea, R. Tasseff, R. Isfort, C. Bascom, T. von Zglinicki and S. Przyborski, *Aging Cell*, 2022, **21**, e13550.
17 I. Lämmermann, L. Terlecki-Zaniewicz, R. Weinmüllner, M. Schosserer, H. Dellago, A. D. de Matos Branco, D. Autheried, B. Sevcnikar, L. Kleissl, I. Berlin, F. Morizot, F. Lejeune, N. Fuzzati, S. Forestier, A. Toribio, A. Tromeur, L. Weinberg, J. C. Higareda Almaraz, M. Scheideler, M. Rietveld, A. El Ghalbzouri, E. Tschachler, F. Gruber and J. Grillari, *npj Aging Mech. Dis.*, 2018, **4**, 4.
18 S. Jeong, J. Kim, H. M. Jeon, K. Kim and G. Y. Sung, *Int. J. Mol. Sci.*, 2021, **22**, 12788.
19 S. N. Mowla, E. W.-F. Lam and P. S. Jat, *Aging Cell*, 2014, **13**, 773–779.
20 W. Lee, J. C. Debasitis, V. K. Lee, J.-H. Lee, K. Fischer, K. Edminster, J.-K. Park and S.-S. Yoo, *Biomaterials*, 2009, **30**, 1587–1595.
21 T. Baltazar, J. Merola, C. Catarino, C. B. Xie, N. C. Kirkiles-Smith, V. Lee, S. Hotta, G. Dai, X. Xu, F. C. Ferreira, W. M. Saltzman, J. S. Pober and P. Karande, *Tissue Eng., Part A*, 2020, **26**, 227–238.
22 V. J. Cristofalo and R. J. Pignolo, *Physiol. Rev.*, 1993, **73**, 617–638.
23 S. Goldstein, *Science*, 1990, **249**(4973), 1129–1133.

Published on 14 July 2025. Downloaded by Indian Institute of Technology New Delhi on 8/9/2025 1:57:37 AM.

24 J. C. Angello, W. R. Pendergrass, T. H. Norwood and J. Prothero, *J. Cell. Physiol.*, 1989, **140**(2), 288–294.
25 D. Asselineau, S. Ricois, H. Pageon, H. Zucchi, S. Girardeau-Hubert, C. Deneuville, V. Haydont, V. Neiveyans and I. Lorthois, *Textbook of Aging Skin*, 2017, 1203–1228.
26 J. Malda, J. Visser, F. P. Melchels, T. Jüngst, W. E. Hennink, W. J. A. Dhert, J. Groll and D. W. Hutmacher, *Adv. Mater.*, 2013, **25**, 5011–5028.
27 W. L. Ng, S. Wang, W. Y. Yeong and M. W. Naing, *Trends Biotechnol.*, 2016, **34**, 689–699.
28 P. Benny, C. Badowski, E. B. Lane and M. Raghunath, *Tissue Eng., Part A*, 2015, **21**, 183–192.
29 S. Vijayavenkataraman, W.-C. Yan, W. F. Lu, C.-H. Wang and J. Y. H. Fuh, *Adv. Drug Delivery Rev.*, 2018, **132**, 296–332.
30 M. Hosseini and A. Shafiee, *Small*, 2021, **17**, e2101384.
31 P. Admane, A. C. Gupta, P. Jois, S. Roy, C. Chandrasekharan Lakshmanan, G. Kalsi, B. Bandyopadhyay and S. Ghosh, *Bioprinting*, 2019, **15**, e00051.
32 I. Ben-Porath and R. A. Weinberg, *Int. J. Biochem. Cell Biol.*, 2005, **37**(5), 961–976.
33 Z. Wang, D. Wei and H. Xiao, *Methods Mol. Biol.*, 2013, **1048**, 135–144.
34 I. A. Gamaley and I. V. Klyubin, *Int. Rev. Cytol.*, 1999, **188**, 203–255.
35 Q. Chen and B. N. Ames, *Proc. Natl. Acad. Sci. U. S. A.*, 1994, **91**(10), 4130–4134.
36 J. Duan, J. Duan, Z. Zhang and T. Tong, *Int. J. Biochem. Cell Biol.*, 2005, **37**(7), 1407–1420.
37 S. R. K. Seshasai, S. Kaptoge, A. Thompson, E. Di Angelantonio, P. Gao, N. Sarwar, P. H. Whincup, K. J. Mukamal, R. F. Gillum, I. Holme, I. Njølstad, A. Fletcher, P. Nilsson, S. Lewington, R. Collins, V. Gudnason, S. G. Thompson, N. Sattar, E. Selvin, F. B. Hu and J. Danesh, *N. Engl. J. Med.*, 2011, **364**(9), 829–841.
38 S. Blazer, E. Khankin, Y. Segev, R. Ofir, M. Yalon-Hacohen, Z. Kra-Oz, Y. Gottfried, S. Larisch and K. L. Skorecki, *Biochem. Biophys. Res. Commun.*, 2002, **296**(1), 93–101.
39 J. Chintapalli, S. Yang, D. Opawumi, S. R. Goyal, N. Shamsuddin, A. Malhotra, K. Reiss and L. G. Meggs, *Am. J. Physiol.*, 2007, **292**(2), F523–F530.
40 R. Noordam, D. A. Gunn, C. C. Tomlin, A. B. Maier, S. P. Mooijaart, P. E. Slagboom, R. G. J. Westendorp, A. J. M. De Craen and D. Van Heemst, *Age*, 2013, **35**(1), 189–195.
41 D. A. Gunn, H. Rexbye, C. E. M. Griffiths, P. G. Murray, A. Fereday, S. D. Catt, C. C. Tomlin, B. H. Strongitharm, D. I. Perrett, M. Catt, A. E. Mayes, A. G. Messenger, M. R. Green, F. van der Ouderaa, J. W. Vaupel and K. Christensen, *PLoS One*, 2009, **4**(12), e8021.
42 J. Chakraborty, J. Fernández-Pérez, M. Takhsha Ghahfarokhi, K. A. van Kampen, T. ten Brink, J. Ramis, M. Kalogeropoulou, R. Cabassi, C. de Julián Fernández, F. Albertini, C. Mota, S. Ghosh and L. Moroni, *Cell Rep. Phys. Sci.*, 2024, **5**, 101819.
43 S. Bruno, M. B. Herrera Sanchez, C. Pasquino, M. Tapparo, M. Cedrino, C. Tetta and G. Camussi, *Stem Cells Int.*, 2019, e6351091.
44 A. C. Gupta, S. Chawla, A. Hegde, D. Singh, B. Bandyopadhyay, C. C. Lakshmanan, G. Kalsi and S. Ghosh, *J. Cell. Physiol.*, 2018, **233**(11), 9015–9030.
45 S. Chawla and S. Ghosh, *Acta Biomater.*, 2018, **69**, 131–145.
46 S. Chawla and S. Ghosh, *J. Cell. Physiol.*, 2018, **233**, 3817–3830.
47 B. Snel, G. Lehmann, P. Bork and M. A. Huynen, *Nucleic Acids Res.*, 2000, **28**, 3442–3444.
48 G. P. Dimri, X. Lee, G. Basile, M. Acosta, G. Scott, C. Roskelley, E. E. Medrano, M. Linskens, I. Rubelj, O. Pereira-Smith, M. Peacocke and J. Campisi, *Proc. Natl. Acad. Sci. U. S. A.*, 1995, **92**, 9363–9367.
49 K. J. Livak and T. D. Schmittgen, *Methods*, 2001, **25**(4), 402–408.
50 M. Nakamura, T. Haarmann-Stemmann, J. Krutmann and A. Morita, *Exp. Dermatol.*, 2018, **27**, 495–500.
51 M. Aleemardani, M. Z. Trikić, N. H. Green and F. Claeyssens, *Bioengineering*, 2021, **8**, 148.
52 Y. Liu, J. Schwam and Q. Chen, *Cells*, 2022, **11**, 1089.
53 V. Gorgoulis, P. D. Adams, A. Alimonti, D. C. Bennett, O. Bischof, C. Bishop, J. Campisi, M. Collado, K. Evangelou, G. Ferbeyre, J. Gil, E. Hara, V. Krizhanovsky, D. Jurk, A. B. Maier, M. Narita, L. Niedernhofer, J. F. Passos, P. D. Robbins, C. A. Schmitt, J. Sedivy, K. Vougas, T. von Zglinicki, D. Zhou, M. Serrano and M. Demaria, *Cell*, 2019, **179**, 813–827.
54 Q. M. Chen, V. C. Tu, J. Catania, M. Burton, O. Toussaint and T. Dilley, *J. Cell Sci.*, 2000, **113**, 4087–4097.
55 B. Y. Lee, J. A. Han, J. S. Im, A. Morrone, K. Johung, E. C. Goodwin, W. J. Kleijer, D. DiMaio and E. S. Hwang, *Aging Cell*, 2006, **5**, 187–195.
56 E. S. Hwang, G. Yoon and H. T. Kang, *Cell. Mol. Life Sci.*, 2009, **66**(15), 2503.
57 S. Atkuru, G. Muniraj, T. Sudhaharan, K.-H. Chiam, G. D. Wright and G. Sriram, *J. Periodontal Res.*, 2021, **56**, 108–120.
58 B. Russo, N. C. Brembilla and C. Chizzolini, *Front. Immunol.*, 2020, **11**, 648.
59 M. Yaar and B. A. Gilchrest, *Clin. Exp. Dermatol.*, 2001, **26**, 583–591.
60 J. Diekmann, L. Alili, O. Scholz, M. Giesen, O. Holtkötter and P. Brenneisen, *Exp. Dermatol.*, 2016, **25**, 56–61.
61 T. Sakai, M. Larsen and K. M. Yamada, *Nature*, 2003, **423**, 876–881.
62 L. Lukjanenko, M. J. Jung, N. Hegde, C. Perruisseau-Carrier, E. Migliavacca, M. Rozo, S. Karaz, G. Jacot, M. Schmidt, L. Li, S. Metairon, F. Raymond, U. Lee, F. Sizzano, D. H. Wilson, N. A. Dumont, A. Palini, R. Fässler, P. Steiner, P. Descombes, M. A. Rudnicki, C.-M. Fan, J. von Maltzahn, J. N. Feige and C. F. Bentzinger, *Nat. Med.*, 2016, **22**, 897–905.
63 G. J. Fisher, J. Varani and J. J. Voorhees, *Arch. Dermatol.*, 2008, **144**(5), 666–672.
64 J. Varani, M. K. Dame, L. Rittie, S. E. G. Fligiel, S. Kang, G. J. Fisher and J. J. Voorhees, *Am. J. Pathol.*, 2006, **168**(6), 1861–1868.
65 G. Theocharidis and J. T. Connelly, *J. Anat.*, 2019, **235**, 249–418.
66 M. A. Cole, T. Quan, J. J. Voorhees and G. J. Fisher, *J. Cell Commun. Signal.*, 2018, **12**(1), 35–43.

 This journal is © The Royal Society of Chemistry 2025

Published on 14 July 2025. Downloaded by Indian Institute of Technology New Delhi on 8/9/2025 1:57:37 AM.

67 K. Oender, A. Trost, C. Lanschuetzer, M. Laimer, M. Emberger, M. Breitenbach, K. Richter, H. Hintner and J. Bauer, *Mech. Ageing Dev.*, 2008, **129**, 563–571.
68 M. Moravcová, A. Libra, J. Dvořáková, A. Víšková, T. Muthný, V. Velebný and L. Kubala, *Interdiscip. Toxicol.*, 2013, **6**, 203–208.
69 M. A. Schwartz, *Old Spring Harb. Perspect Biol.*, 2010, **2**(12), a005066.
70 M. A. Wozniak, K. Modzelewska, L. Kwong and P. J. Keely, *Biochim. Biophys. Acta*, 2004, **1692**(2–3), 103–119.
71 A. L. Plant, K. Bhadriraju, T. A. Spurlin and J. T. Elliott, *Biochim. Biophys. Acta, Mol. Cell Res.*, 2009, **1793**, 893–902.
72 K. M. K. Rao and H. J. Cohen, *Mutat. Res., DNAging: Genet. Instab. Aging*, 1991, **256**(2–6), 139–148.
73 C. Schulze, F. Wetzel, T. Kueper, A. Malsen, G. Muhr, S. Jaspers, T. Blatt, K. P. Wittern, H. Wenck and J. A. Käs, *Clin. Plast. Surg.*, 2012, **39**(1), 9–20.
74 L. I. Pease, J. Wordsworth and D. Shanley, *bioRxiv*, 2022, DOI: **10.1101/2022.08.16.504111**.
75 T. Ide, W. K. Twan, H. Lu, Y. Ikawa, L.-X. Lim, N. Henninger, H. Nishimura, K. Takaoka, V. Narasimhan, X. Yan, H. Shiratori, S. Roy and H. Hamada, *PLoS Genet.*, 2020, **16**, e1009232.
76 V. Kumar, K. C. Bermea, D. Kumar, A. Singh, A. Verma, M. Kaileh, R. Sen, E. G. Lakatta and L. Adamo, *Geroscience*, 2024, **46**, 4243–4262.
77 R. Anderson and T. Prolla, *Biochim. Biophys. Acta*, 2009, **1790**, 1059–1066.
78 A. A. Batavia, D. Rutishauser, B. Sobottka, P. Schraml, N. Beerenwinkel and H. Moch, *Mod. Pathol.*, 2023, **36**, 100194.
79 S. Kleiser and A. Nyström, *Biomolecules*, 2020, **10**, 1170.
80 J. Chaudhuri, Y. Bains, S. Guha, A. Kahn, D. Hall, N. Bose, A. Gugliucci and P. Kapahi, *Cell Metab.*, 2018, **28**, 337–352.
81 H. Hooi Ng, M. Shen, C. S. Samuel, J. Schlossmann and R. G. Bennett, *Mol. Cell. Endocrinol.*, 2019, **487**, 59–65.
82 Q. M. Chen, V. C. Tu and J. Liu, *Biogerontology*, 2000, **1**, 335–339.
83 M. Gülden, A. Jess, J. Kammann, E. Maser and H. Seibert, *Free Radicals Biol. Med.*, 2010, **49**(8), 1298–1305.
84 J. Jin and T. Zhang, *Cell. Physiol. Biochem.*, 2013, **31**(4–5), 718–727.
85 D. Kido, K. Mizutani, K. Takeda, R. Mikami, T. Matsuura, K. Iwasaki and Y. Izumi, *PLoS One*, 2017, **12**(12), e0189601.
86 L. Pang, Y. Wang, M. Zheng, Q. Wang, H. Lin, L. Zhang and L. Wu, *Mol. Med. Rep.*, 2016, **13**, 2627–2634.
87 P. Buranasin, K. Mizutani, K. Iwasaki, C. P. N. Mahasarakham, D. Kido, K. Takeda and Y. Izumi, *PLoS One*, 2018, **13**(8), e0201855.
88 K. D. Salpea, P. J. Talmud, J. A. Cooper, C. G. Maubaret, J. W. Stephens, K. Abelak and S. E. Humphries, *Atherosclerosis*, 2010, **209**(1), 42–50.
89 B. Li, X. Bian, W. Hu, X. Wang, Q. Li, F. Wang, M. Sun, K. Ma, C. Zhang, J. Chang and X. Fu, *Wound Repair Regen.*, 2020, **28**(3), 315–325.
90 A. Di Leonardo, S. P. Linke, K. Clarkin and G. M. Wahl, *Genes Dev.*, 1994, **8**(21), 2540–2551.
91 W. Wharton, *Cancer Res.*, 1995, **55**, 5069–5074.
92 C. Frippiat, J. Dewelle, J. Remacle and O. Toussaint, *Free Radicals Biol. Med.*, 2002, **33**(10), 1334–1346.
93 T. Y. McCarty and C. J. Kearney, *Front. Aging*, 2025, **6**, 1504977.